BEST AVAILABLE COPY

AD 681 533

CONE CAVITY FLOW AT M=5.3 WITH INJECTION OF LIGHT, MEDIUM AND HEAVY GASES

Jean J. Ginoux, et al

von Karman Institute for Fluid Dynamics
Rhode-Saint-Genese, Belgium

November 1968

AFOSR 69-0168TR

BEST AVAILABLE COPY

VKI TN 35

von KARMAN INSTITUTE

FOR FLUID DYNAMICS

GRANT AF EOOAR 68-003
Final Scientific Report
1 October 1967 - 30 September 1968
(Laminar Separation at Hypersonic Speeds)
CR-68-Gi-I-2

AD681533

CONE CAVITY FLOW AT M = 5.3 WITH INJECTION OF LIGHT, MEDIUM AND HEAVY GASES

by

Jean J. GINOUX

and

Félix THIRY

VKI TN 35

This document has been approved for public release and sale; its distribution is unlimited

RHODE-SAINT-GENESE, BELGIUM

NOVEMBER 1968

FEB 5 1969

Reproduced by the
CLEARINGHOUSE
for Federal Scientific & Technical
Information Springfield Va. 22151

55

BEST AVAILABLE COPY

GRANT AF EOOAR 68-003 November 1968

FINAL SCIENTIFIC REPORT

LAMINAR SEPARATION AT HYPERSONIC SPEEDS

1 October 1967 - 30 September 1968

Jean J. GINOUX

and

Félix THIRY

von Karman Institute for Fluid Dynamics
Rhode Saint Genèse, Belgium

Technical Note 35

This document has been approved for public release and sale; its distribution is unlimited

This research has been sponsored in part by the Air Force Office of Scientific Research, through the European Office of Aerospace Research, OAR, United States Air Force, under Grant AF EOOAR 68-003.

TABLE OF CONTENTS

SUMMARY ii
LIST OF FIGURES iii
NOTATIONS iv

1. INTRODUCTION 1
2. EXPERIMENTAL EQUIPMENT AND TEST TECHNIQUES 2
   2.1 Wind tunnel 2
   2.2 Models 2
   2.3 Model adjustment 3
   2.4 Heat transfer technique 4
   2.5 Injection plant 5
3. RESULTS AND DISCUSSION 7
   3.1 Flow visualization 7
   3.2 Pressure measurements 10
   3.3 Heat transfer measurements 14
4. CONCLUSIONS 17

REFERENCES 18
TABLE I 20
FIGURES

BEST AVAILABLE COPY

SUMMARY

The effect on the reattachment pressure and heat transfer peaks of injection of air and foreign gases into the separated region of the laminar flow over a cone cavity model has been investigated at M = 5.3.

Injection has generally a favorable effect in reducing these peaks, light gases being more effective. A correlation factor is given to relate together the effects of various gases. A surprizing similarity is found with theoretical and experimental results for unseparated flows over porous walls. Occasionally, very high frequency flow unsteadiness has been observed.

BEST AVAILABLE COPY

LIST OF FIGURES

1 Model configurations : a. Pressure model
b. Heat transfer model

2 Control plant for gas injection

3 Pressure distributions with and without gas injection
a. Hydrogen
b. Helium
c. Air
d. Freon
e. Carbon tetrachloride

4 Average heat transfer distribution without gas injection

5 Heat transfer distributions with and without gas injection : a. Hydrogen
b. Helium
c. Air
d. Freon

6 Schlieren photographs for air injection

7 Shadowgraphs for air injection

8 Shadowgraphs for freon injection

9 Visualization of flow unsteadiness

10 Supersonic flow over a rectangular cavity

11 Effect of gas injection on maximum pressure ratio

12 Effect of gas injection on maximum heat transfer ratio

13 Correlated pressure and heat transfer peak ratios

14 Correlation factor K versus molecular weight

15 Comparison between pressure and heat flux distributions ($c_q = 0$)

NOTATIONS

c	specific heat of model skin material
c_q	injection rate coefficient; $c_q = Q_{inj}/Q_{BL}$
d	skin thickness of heat transfer model
K	correlation factor
L	cavity width
M	molecular weight of injected gas
p	static pressure
p_c	cone pressure
q	heat transfer per unit area and unit time
q_c	heat transfer on a cone
Q_{inj}	mass flow injected into the cavity
Q_{BL}	mass flow in the boundary layer at separation
t	time
T	temperature
T_w	skin temperature
x	curvilinear coordinate with its origin defined in the sketch on page 10
ρ	density of model skin material
θ	azimuth of pressure taps or thermocouples (fig.1a-1b)

1. INTRODUCTION

For a number of years, it has been known that the presence of a cavity in the surface of a hypersonic body gives rise to a significant redistribution of surface pressure and heat transfer to the body (refs 1,2,3). Specifically, these quantities are reduced in the region of separated flow, but experience a sharp increase within the vicinity of reattachment, followed by a decrease toward the undisturbed values in the downstream area. For practical applications, the primary undesirable feature of this phenomenon is the elevated pressure and heat transfer at reattachment. This fact justifies further research into methods of substantially reducing these peak values.

In this regard, it has been previously theoretically predicted and experimentally verified that injection of a small amount of gas (a fraction of the mass flow in the boundary layer at separation is sufficient) into the separated region accomplishes this result (refs 1,4,5,6).

The investigation of reference 6 was directed toward provision of detailed static pressure and heat transfer distributions over the entire surface of cone-cavity models with and without air injection into the cavity at a free stream Mach number of 5.3. Emphasis was given to the reattachment region by using a cavity with a rounded reattachment shoulder, as opposed to Nicoll's cavity which had 90° sharp corners.

The present study is an extension of the work done in reference 6 whereby the effect of foreign gas injection has been included. Light gases (helium and hydrogen) and heavy gases (freon and carbon tetrachloride vapor) were used in addition to air as previously tested.

2. EXPERIMENTAL EQUIPMENT AND TEST TECHNIQUES

2.1 Wind tunnel

All experiments were conducted in the VKI hypersonic blowdown tunnel H-1 at a free stream Mach number of 5.3. The size of the test section is 12×12 cm^2, giving a uniform flow with $\pm \frac{1}{2}$ percent variation in Mach number. The stagnation temperature was about 220°C. The stagnation pressure was 15 atms, corresponding to a free stream Reynolds number of 1.62×10^5 per centimeter.

2.2 Models

The basic model configuration is a 10° semi-apex angle cone incorporating an annular cavity of the short-deep type. The pressure and heat transfer models are shown in figures 1a and 1b respectively. Dimensions are in millimeters and one should note the slight differences in nose length and cavity width of the two models. The radius of the rounded reattachment shoulder is equal to 4 mm.

The locations of the pressure taps and thermocouples are given in the tables shown in these figures. x in millimeters is the curvilinear coordinate along the model generator, with its origin at the junction between the shoulder and the after-cone (see sketch on page 10). After machining, this junction was difficult to locate relatively to the pressure taps or thermocouples and, as a result, an error of 0.1 to 0.2 mm is possible on all the x-coordinates for each of the two models. The detailed determination of reattachment pressure and heat transfer rises required that several sensors (pressure taps or thermocouples) be located within a distance of 6 millimeters in the vicinity of reattachment. In order to do so, they had to be staggered by

an angle θ given in the tables of figures 1a,1b. Three pressure taps (# 1,2,3) are not indicated in figure 1a. # 1 was located on the forecone, 20 mm upstream of the cavity and was used to measure the cone pressure to which all the other measured pressures were referred. Pressure taps # 2,3 were inside the cavity.

The injected gas entered the cavity tangentially to the floor from an annular port (1 mm wide) located at the base of the reattachment shoulder. The interior of the models was designed in such a way that the measured velocity variations at the slot exit were smaller than one percent.

The pressure model was designed with 0.45 mm inner diameter tubing connected to 12-tube rotary valves and a differential transducer. The output of the transducer was recorded by a digital printer giving three significant figures.

2.3 Model adjustment

In reference 6, each of the two models was adjusted to zero incidence and yaw by using a set of four alignment pressure taps located at a single axial station three cavity widths upstream of the model base and spaced 90° apart. However, it was later discovered that under these conditions the reattachment pressure and heat transfer peaks did not remain constant when the models were rotated by 90 and 180 degrees around their axes, but varied by about 12 percent. This was due to small non-uniformities in the free stream.

For this reason, in the present study, the incidence and yaw were adjusted in order to measure the same peaks (either pressure or heat transfer) at the 0, 90 and 180 degrees azimuthal positions.

BEST AVAILABLE COPY

2.4 Heat transfer technique

Heat transfer rates were measured by the thin skin technique. The heat transfer model, machined from stainless steel is the same as used in reference 6. Its skin thickness varies from 0.5 to 0.6 mm (instead of 0.8 mm as incorrectly measured in reference 6). Copper constantan wires of 0.06 and 0.1 mm diameters were inserted into 0.25 mm holes drilled through the model skin and soldered.

The model, initially at room temperature, was suddenly exposed to the air stream when the hypersonic tunnel was started using a quick opening valve. The temperature-time histories as well as the tunnel stagnation temperature were measured on a 15-channel CEC galvanometric recorder. The heat flux to the model surface per unit area and unit time was computed from the equation

$$q = \rho c d^{M} \frac{\partial T}{\partial t}$$

where $\rho = 7.68$ gr/cm^3 and $c = 0.114$ cal/gr.deg are the density and specific heat of the stainless steel used to fabricate the model skin. d^M is the effective skin thickness, i.e. the measured thickness (d) multiplied by a correction factor function of the local geometry of the model; either a torus for the reattachment shoulder or a cone further downstream. $\frac{\partial T}{\partial t}$ is the temperature-time derivative measured, for each of the thermocouples, approximately 0.1 second after the tunnel was started. At that time, the model temperature (T_w) was still uniform and equal to the room temperature; thus, no correction for transverse heat conduction along the skin was attempted.

The measured heat flux (q) was referred to the theoretical pure cone value (q_c) evaluated at the same distance from

the model nose. The cone temperature was taken equal to T_w. The recovery temperature was calculated from a constant recovery factor equal to 0.83, verified experimentally, and the stagnation temperature measured at the same time as $\frac{\partial T}{\partial t}$ was recorded. The stagnation temperature did not always rise monotonously when the tunnel was started, but often reached a plateau for a very short time interval, during which $\frac{\partial T}{\partial t}$ was recorded, before reaching its final value. In these conditions, the plateau value was used in the data reduction rather than the final value which was approximately 10 to 20 degrees higher.

2.5 Injection plant

The gases used in the present investigation are identified in table I. The injection plant, used to supply precise amounts of these gases to the plenum chamber of the cavity model, is schematically shown in figure 2. It consists of two parts; part (a) is used for the injection of dry air, freon, helium or hydrogen and part (b) is used for the injection of carbon tetrachloride which is liquid under standard atmospheric conditions.

In part (a) of the injection plant, the gas flows through a sonic orifice disc so that the injection rate is essentially proportional to the stagnation tank pressure which is controlled manually by a needle valve. To cover the ranges of mass injection rates desired for the various gases, several interchangeable orifice discs were necessary. These were calibrated by maintaining a constant tank pressure while the gas passed, for a measured amount of time into a downstream tank of known volume, initially evacuated. By measuring the initial and final pressures and temperatures in the downstream reservoir the mass flow could be accurately calculated.

In part (b), carbon tetrachloride is boiling at 76.8°C under atmospheric pressure in a boiler (1). The vapor, which is maintained hot in a water tank (9), flows through a diaphragm (7) and then expands through a manually operated needle valve (2) which controls the mass flow. Initially, air is evacuated from the injection plant by means of a vacuum pump (3). When pure carbon tetrachloride vapor reaches the condenser (4), a partial vacuum is automatically maintained after switching off the vacuum pump. Just before starting the tunnel, a supersonic ejector is used to reduce the pressure in the tunnel diffuser and test section to about one tenth of an atmosphere. Then valve (5) is opened and valve (6) closed. The gas is then driven through the system by the low pressure that exists in the model cavity. After starting the tunnel, the cavity pressure further decreases and the rate of gas injection remains the same. The mass flow is measured by a calibrated diaphragm (7) and a pressure transducer. Its calibration was made as described for part (a) of the injection plant.

In this report, the injection rate is normalized with the theoretical air mass flow rate (Q_{BL}) in the boundary layer at separation:

$$c_q = \frac{Q_{inj}}{Q_{BL}}$$

Q_{BL} was calculated from the theory of Chapman and Rubesin after applying a Mangler transformation. It was based on the stagnation conditions measured in each of the tests. Q_{BL} was equal to 21.7 liters/minute, based on standard conditions, for stagnation conditions such as 220°C and 15 atms assuming a wall temperature of 80°C for the pressure model and 22.2 liters/minute under the same conditions for the heat transfer model at a wall temperature of 27°C. c_q was varied in the tests in steps over

different ranges for the different gases, such as zero to 0.1 for hydrogen, zero to 0.45 for air, etc.

It was impossible to inject gas into the cavity with zero momentum. Calculation shows for instance that, at a value of c_q of one quarter for air (which is sufficient to suppress the reattachment pressure and heat transfer peaks), the injected momentum was of three percent of the momentum contained in the boundary layer at separation. This is sufficiently small to have none but little effect on the flow. It was indeed confirmed by the fact that the pressure distribution did not change when, in a separate test, air was injected normally to the cavity floor through a series of small holes. However, it is possible that such an effect exists when light gases are injected. Indeed at a value of c_q equal to one quarter, the injected momentum of hydrogen is approximately half that of air in the boundary layer at separation.

3. RESULTS AND DISCUSSION

3.1 Flow visualization

Typical schlieren and shadow photographs of the flow over the cavity model are presented in figures 6,7 and 8 for various injection rates. They show the following results:

At $c_q = 0$ (no injection), an expansion fan exists at separation and a shock appears at reattachment, in agreement with the pressure data of figure 3 (the measured cavity pressure is lower than the cone pressure). With increasing injection rate, the separation expansion and reattachment shock both

diminish in intensity. At a certain value of c_q, the separation expansion completely disappears and at higher injection rates it is replaced by a separation shock. For air, figure 3 shows that this value of c_q is of about 0.13. The reattachment shock becomes very weak but never disappears. It moves slightly forward for higher injection rates, which corresponds to the upstream displacement of the pressure peak seen in figure 3.

At $c_q = 0$, the flow is laminar over most of the body surface; transition is located approximately ten millimeters upstream of the base (i.e., at $\frac{x}{L} = 6$). With increasing injection of air or light gases, transition seems to remain fixed first and then travels upstream. With freon injection, transition first moves downstream. This is seen by comparing the photographs of figures 8a to 8d. For $c_q = 0$, transition is 10 to 15 millimeters upstream of the base while at values of c_q up to .22 there is no indication of transition over the entire model surface. Then for an injection rate of .28 transition again appears (figure 8d) near the model base.

At large values of c_q, such as 0.7 for air, transition is located approximately one or two cavity lengths downstream of reattachment. This explains, in figures 5a to 5d, the increase in heat transfer for $\frac{x}{L}$ larger than one to two at large values of c_q.

Occasionally a third shock, located between the separation and reattachment shocks, was observed on the flow pictures, particularly at large injection rates of light gases. This shock is rooted in the free shear layer. A typical example is shown for the case of helium injection in figure 9a. With light gas injection, the velocity at the exit of the injection slot becomes large (sonic) and it is possible that a high speed jet forms

which hits the free shear layer in the region where the third shock appears. However, such a high speed jet was never visible on the flow pictures.

Another possible explanation can be obtained from the observation that the flow over the cavity appeared to be unsteady in some cases. This can be seen in figure 9a or its enlargement shown in figure 9b. Indeed, the bright line which is characteristic of a laminar type boundary layer, is rather wavy downstream of the cavity. This suggests the existence of periodic pressure fluctuations in the cavity. The frequencies were estimated to be of order 5×10^5 Hz. To further substantiate this, two schlieren pictures of a supersonic flow over a cavity are shown in figure 10. They were taken by the authors in the VKI supersonic tunnel S-1 at a free stream Mach number of 2.2 in the course of a previous unpublished study. One of the pictures (10a) is taken with a spark light source with an exposure time of a few microseconds and it shows the wave pattern produced by the flow unsteadiness. Hot wire measurements made in the cavity indicated that the frequency of the oscillations was of about 10 to 15 thousands cycles per second. The second photograph (fig. 10b) represents the same flow with a longer exposure time ($\frac{1}{50}$ sec). It reveals only the envelopes of the unsteady waves whose number was found to depend upon the cavity width. These envelopes are rooted in the free shear layer exactly like the "third shock" observed in the present study.

It is thus possible that the third shock observed in the present study is the envelope of unsteady waves emitted from an oscillating free shear later and, although the shadowgraphs were taken with only one millisecond exposure time, the frequency of the oscillations was so much higher than in the supersonic case that only the envelope of the waves was visible.

3.2 Pressure measurements

The static pressure distributions measured without injection ($c_q = 0$) and with injection of five different gases are shown in figures 3a to 3e. In these figures, the static pressure is referred to the cone pressure (p_c) measured on the forecone, 20 millimeters downstream of the nose. L is the cavity width (i.e. 12 mm) and x is the surface distance measured along a model generator with its origin at the junction (R) of the reattachment shoulder and the afterbody, as shown in the sketch.

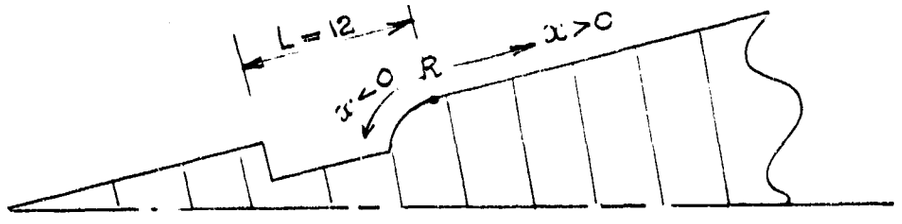

c_q is the ratio of injected mass flow to the boundary layer mass flow computed at separation. The pressure measured inside the cavity is shown on the left side of the graphs. Smooth curves are fitted through the experimental points in the reattachment region and further downstream up to $\frac{x}{L}$ of about 0.8.

Cross plots of figures 3a to 3e are presented in figure 11. They show the variation of reattachment pressure peak with mass injection rate.

From these figures, a number of observations can be made which illustrate the character of the flow phenomenona involved.

With zero injection, the cavity floor pressure is ten percent below cone pressure. The static pressure rises over the cavity shoulder and reaches a maximum which is 59% higher than cone pressure, approximately 0.5 mm upstream of the junction ($x = 0$) between the shoulder and the aftercone. The existence of a pressure peak can be physically justified by Chapman's criteria of mass conservation inside the cavity. Indeed, a pressure rise must exist at reattachment in order to return into the cavity the fluid which has been entrained by mixing with the shear layer. Thus as the cavity pressure is slightly lower than cone pressure, the pressure must necessarily peak up above the cone pressure. Figures 3 shows that, downstream of the peak, the pressure drops first rapidly and then very slowly towards cone pressure.

Now considering the case of no-zero mass injection, it is seen from figures 3a to 3e that the cavity floor pressure increases gradually with injection and becomes higher than cone pressure, while there is a general decrease of the pressure level in the reattachment region. The reattachment pressure peak shown in figure 11, decreases sharply and linearly with increasing injection while remainig at a fixed position ($\frac{x}{L} = -0.05$). Then, it decreases more slowly while moving upstream, until a region of constant peak pressure, about ten percent higher than cone pressure, is reached. Following this region, the pressure peak increases slightly with additional injection. Physically, by injecting gas into the cavity, part of fluid entrained by the shear layer need not return into the cavity and, therefore, the reattachment pressure rise is reduced with a corresponding reduction of the pressure peak.

Figure 11 shows that the lighter the gas is the larger the rate of decrease of peak pressure is. This is in agreement with theories for incompressible and compressible unseparated

laminar boundary layers with foreign gas injection (see for instance refs 7,8,9). These analyses indeed show that substantial reduction in skin friction and heat transfer can be obtained by injection of light gas instead of air. This means, for practical applications, that less storage weight is required in order to reduce the peak pressure by a given amount when light gases are used. The curves of figure 11 are nearly homothetic. Indeed, they can be approximately superposed by multiplying the abscissa c_q by a constant factor K. This is shown in figure 13, where the maximum pressure ratio is plotted versus $K.c_q$, so that the curves coincide for a pressure ratio equal to 1.35. Coefficient K is the mass flow ratio of foreign gas to air needed to reduce the pressure peak by a given amount. It is plotted in figure 14 against the molecular weight of the gas in logarithmic scale.

In reference (7), Faulders presents some numerical results for the relationship between skin friction and blowing rate for a flat porous plate in the case of laminar incompressible flow without heat transfer. He assumes that the injection velocity varies inversely as the square root of the distance from the plate leading edge. His results show the significant effect of the variation of the density-viscosity product caused by the injection of foreign gas. Skin friction decreases with increasing blowing rate more effectively with light gases than with heavy ones. Faulders curves of skin friction versus blowing rate are nearly linear and it is possible to collapse them together by multiplying the blowing rate by a coefficient K, which represents the mass flow ratio of foreign gas to air needed to reduce the skin friction coefficient by a given amount. Typical values of K, computed from figure 2 of reference 7 are shown in the semi-logarithmic diagram of figure 14. As seen, these values of K nearly fall on the curve drawn through the present experimental data.

In reference 8, Albacete and Glowacki treat numerically the laminar compressible flow over a porous flat plate assuming a blowing rate inversely proportional to the square root of the distance from the plate leading edge. They show that the reduction of skin friction with increasing blowing depends largely on the density-viscosity product of the gas-air mixture at the wall, itself a function of the molecular weight of the injected gas. It appears from their results that Mach number has little effect on the ratio K introduced in the present study.

In reference 9, Craven solves the equations of the steady compressible two dimensional laminar boundary layer with foreign gas injection through a porous wall for arbitrary injection velocity, pressure gradient and wall temperature. He shows that skin friction and heat transfer rate can be substantially reduced by the injection of light gas instead of air. His numerical results show little dependence of the ratio K on Mach number and heat transfer rate. Typical values of K for helium and hydrogen to air ratios are shown in figure 14. They show again surprizingly good agreement with the present experimental data.

In conclusion, foreign gas injection is substantially more effective in reducing the peak pressure at reattachment with light gases than with air or heavier gases. The measured relative effectiveness of foreign gas and air is surprizingly similar to the calculated relative effect of foreign gas and air blowing on skin friction in the case of an attached flow over a porous flat plate for a wide range of Mach numbers, injection velocity distributions and wall temperatures. This seems to indicate that the reattachment peak pressure depends upon the density-viscosity product of air-gas mixture at reattachment.

3.3 Heat transfer measurements

The heat transfer distributions measured without injection ($c_q = 0$) and with injection of four different gases are shown in figures 4 and 5a to 5d. q is the heat flux per unit area and unit time and (q_c) the computed heat flux on a cone without cavity. x is the distance measured along a model generator with its origin at the junction of the reattachment shoulder and the afterbody. For the simplicity of comparison between pressure and heat transfer distributions, a value of L = 12 mm was used although the cavity width on the heat transfer model was effectively equal to 11.5 mm. c_q is the ratio of mass flow injected to the boundary layer mass flow at separation.

Figure 4 shows typical scatter of the heat transfer distributions measured in seven different runs without injection. An average curve, in dotted line, has been drawn through this data and is replotted in each of figures 5a to 5d which give the effect of gas injection. Heat transfer to the cavity floor was always very small and therefore inaccurately measured; for this reason it is not shown in figures 4 and 5.

With zero injection, the heat flux rises along the reattachment shoulder from a low value up to about 1.6 times the cone value approximately at x = 0. (the higher value obtained in reference 6 is due to incorrect measurement of the model skin thickness). For x positive, $\frac{q}{q_c}$ decreases rather rapidly and goes below the cone value as was previously observed by Nicoll (4). Approximately one cavity width downstream of reattachment, it starts to rise very slowly towards the cone value.

The heat transfer peak is nearly equal to the pressure peak, as shown in figure 15 which compares the static pres-

sure and heat transfer distributions without injection. Assuming a constant product of Stanton number by the square root of the local Reynolds number, one can show that $\frac{q}{q_c}$ varies in hypersonic flow like the square root of $\frac{p}{p_c}$. Thus the existence of a pressure peak partly justifies the presence of a heat transfer peak near reattachment. The latter is further amplified and displaced downstream with respect to the pressure peak by the effects of the strong positive and negative pressure gradients on the Stanton number.

With injection, figures 5a to 5d show a decrease of the heat transfer ratio $\frac{q}{q_c}$ over the whole model surface except at larger injection rates when transition has moved sufficiently upstream to increase the heat transfer rate in the region of interest. Ignoring this effect of transition, it is seen that the heat transfer rate becomes smaller than a certain value which depends upon the type of injected gas.

To compare the effectiveness of the various gases, the peak ratio $(\frac{q}{q_c})_{c\ max}$ has been plotted versus c_q in figure 12. It shows that lighter gases are more efficient than heavier ones to reduce heat transfer to the body surface. For instance, a 50-percent reduction in maximum heat transfer ratio requires mass-flow rates for hydrogen, helium, air and freon in the proportion of 0.27:0.56:1.0 and 1.3; or looking at the results in a different way, an injection rate coefficient of $c_q = 0.04$ causes maximum heat transfer ratio reductions of 57, 31, 22 and 15 percent for hydrogen, helium, air and freon respectively. This trend agrees with theory (8,9) except for small wall to free stream temperature ratios (8) when the effect of molecular diameter overcomes the effect of molecular weight.

Curves of figures 12 have been replotted in figure 13 by multiplying the injection rate coefficient (c_q) by a factor (K) so that they coincide for a heat transfer ratio selected arbitrarily equal to unity. Values of K are shown in figure 14. It is seen that they do not differ appreciably from the values of K derived from the pressure measurements. Also seen in figure 14 is the comparatively larger influence of injection on the heat transfer ratio than on the pressure ratio.

Rubesin and Pappas (ref. 10) compute the effect of distributed light gas injection on skin friction and heat transfer for a turbulent incompressible flow over a flat plate. Values of K computed from their results are shown in figure 14 and agree surprizingly well with the present data. This is also true for the experimental results of Pappas and Okuno (ref. 11) for the turbulent heat transfer to a porous cone at M = 4.35.

It is concluded that light gas injection is substantially more effective in reducing the heat transfer peak at reattachment than air or heavy gas injection. The relative effectiveness (K) of various gases is surprizingly similar for the pressure and heat transfer peaks reduction and also for a wide variety of other experimental and theoretical data on unseparated laminar and turbulent flows over porous flat plates or cones.

4. CONCLUSIONS

Results of reference 6 are extended to include the effect of foreign gas injection on static pressure and heat transfer distributions over a cone cavity model at M = 5.3.

The favorable effect of gas injection into the cavity on reducing the aerodynamic heating of the model is reconfirmed; light gases being more effective than air and heavier gases.

The effectiveness of the various gases that were tested, namely, hydrogen, helium, air freon and carbon tetrachloride on reducing reattachment pressure and heat transfer peaks can be correlated by a single factor which is a function of the molecular weight of the injected gas. Values of this factor, calculated from various published theories and experiments for laminar and turbulent unseparated flows, agree surprizingly well with the present data.

At the largest injection rates that were used, very high frequency unsteadiness seems to develop in the cavity flow.

REFERENCES

1. CHAPMAN, D.R.: A theoretical analysis of heat transfer in regions of separated flow.
NACA TN 3792, 1956.

2. LARSON, H.K.: Heat transfer in separated flow.
J.S.A. Vol. 26, pp 731-738, November 1959.

3. NICOLL, K.M.: A study of laminar hypersonic cavity flows.
AIAA Jnl, vol. 2, n° 3, pp 1535-1541, Sept. 1964.

4. NICOLL, K.M.: Mass injection in a hypersonic cavity flow.
ARL 65-90, May 1965.

5. NICOLL, K.M.: An experimental investigation of laminar hypersonic cavity flows. Part II - Heat transfer and recovery factor measurements.
ARL 63-73, January 1964.

6. GINOUX, J.J.: Laminar separation in hypersonic flows.
Grant AF EOAR 67-09, Final Scientific Report,
November 1967.

7. FAULDERS, C.R.: A note on laminar boundary layer skin friction under the influence of foreign gas injection.
J.A.S. Vol. 28, Feb. 1961, Reader's Forum pp 166-67.

8. ALBACETE, L.M. & GLOWACKI, W.J.: Skin friction and heat transfer characteristics of the compressible laminar boundary layer with injection of a light, medium and heavy gas.
NOL TR 66-215, March 1967.

9. CRAVEN, A.H.: The compressible laminar boundary layer with foreign gas injection.
CoA Report n° 155, January 1962.

10. RUBESIN, M.W. & PAPPAS, C.C.: An analysis of the turbulent boundary layer characteristics on a flat plate with distributed light-gas injection.
NACA TN 4149, Feb. 1958.

11. PAPPAS, C.C. & OKUNO, A.F.: Measurement of heat transfer and recovery factor of a compressible turbulent boundary layer on a sharp cone with foreign gas injection.
NASA TN D 2230, April 1964.

Gas	Hydrogen	Helium	Air	Freon 12 Difluordichlor-methan	Carbon tetrachloride
Symbol	H_2	He		CF_2Cl_2	CCl_4
Molecular weight	2.016	4.003	28.97	121	153.84
Collision diameter (Å)	2.915	2.576	3.617	5.12	5.881
Specific heat c_p kcal/kg °C	3.45	1.24	0.24	0.16	0.13
Viscosity coefficient $\mu \times 10^4$ poises (at 300°K)	.92	2.03	1.85	1.34	.99
Heat conductivity coefficient (k) in kcal/m hr °C at 300°K	0.158	0.131	0.0216	0.0097	0.0055

TABLE I

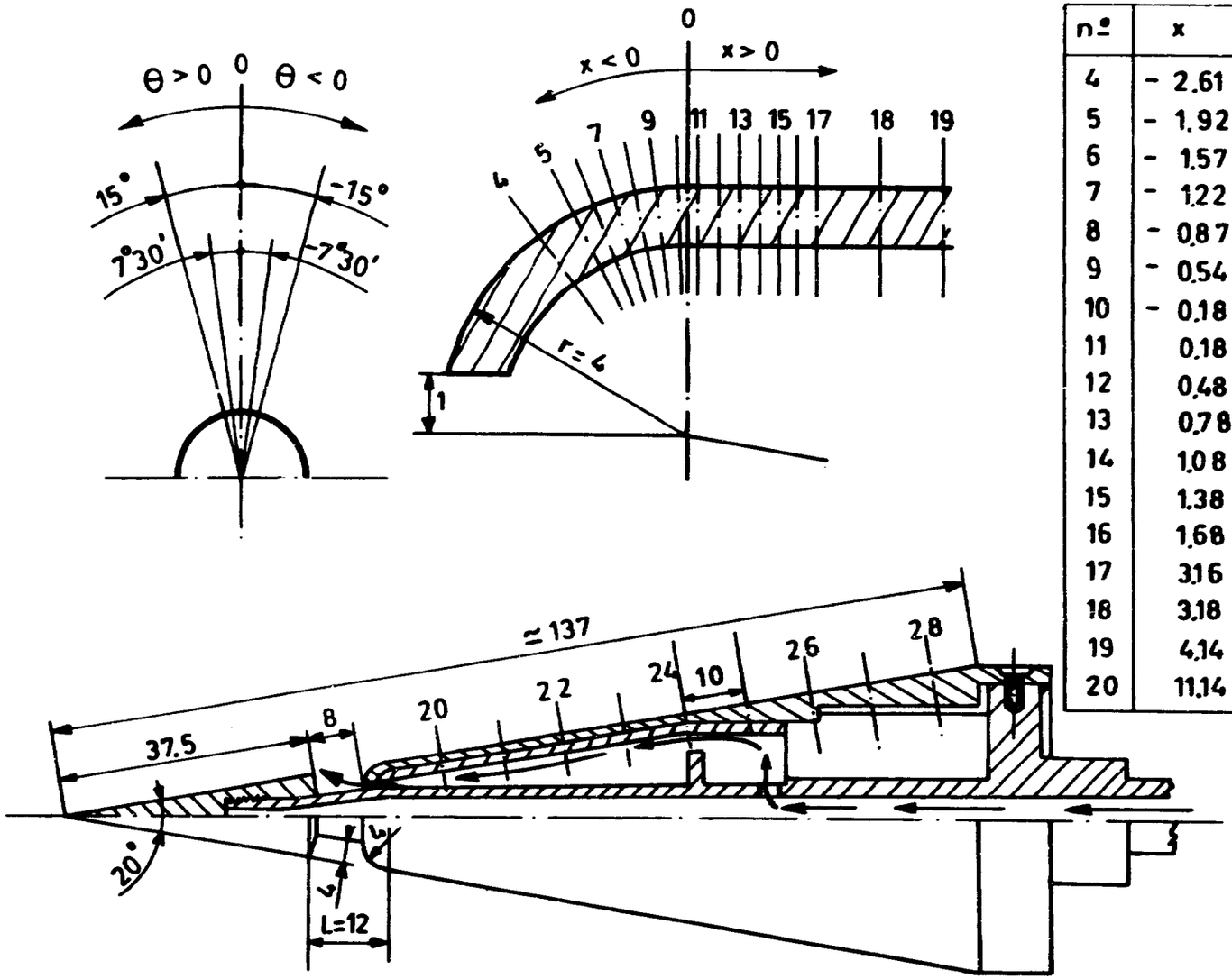

n°	x	θ
4	- 2.61	0
5	- 1.92	15
6	- 1.57	7°30
7	- 1.22	-7°30
8	- 0.87	-15
9	- 0.54	15
10	- 0.18	7°30
11	0.18	-7°30
12	0.48	-15
13	0.78	15
14	1.08	7°30
15	1.38	-7°30
16	1.68	-15
17	3.16	0
18	3.18	0
19	4.14	0
20	11.14	0

a. Pressure model

Fig. 1 MODEL CONFIGURATIONS.

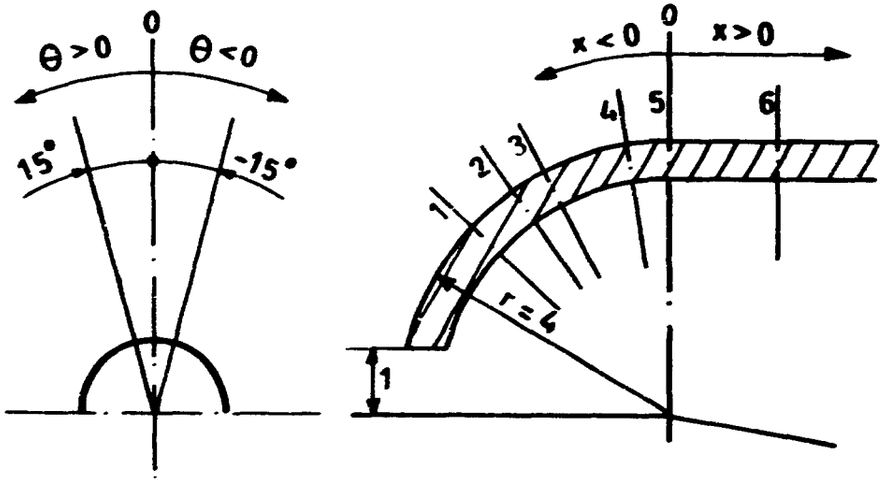

n°	x	θ
1	- 3.30	15
2	- 2.49	0
3	- 1.99	-15
4	- 0.69	15
5	0	0
6	1.59	0
7	3.20	0
8	7.99	0
11	13.20	0
13	23.10	0
14	36.36	0

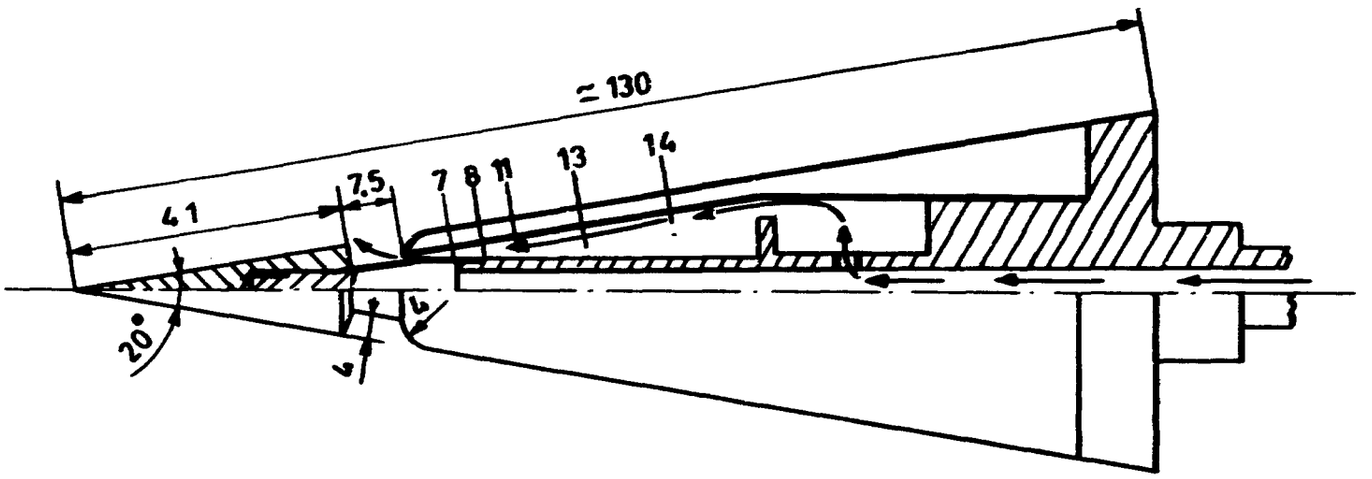

b. Heat transfer model.

Fig. 1 CONCLUDED.

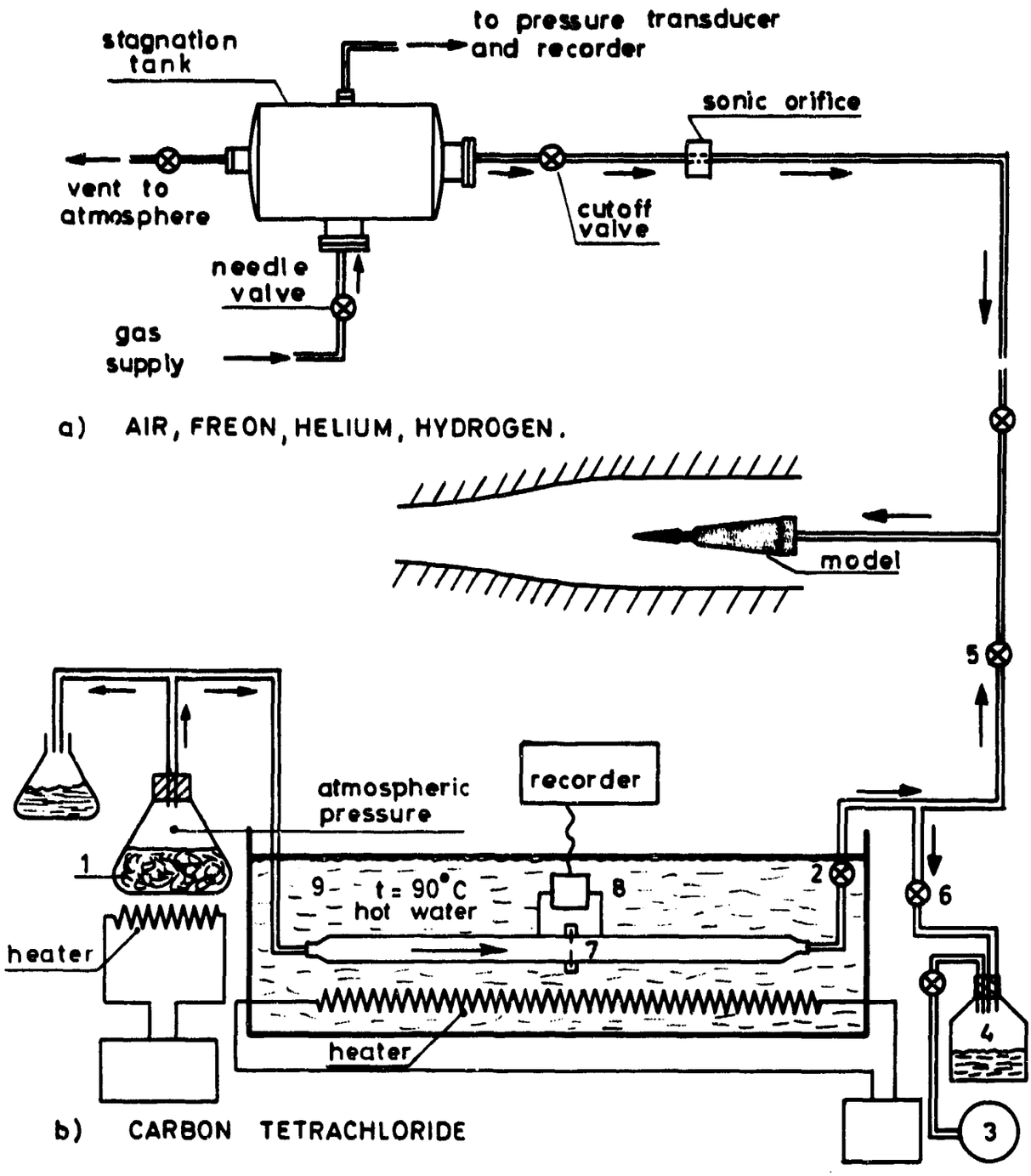

Fig. 2 CONTROL PLANT FOR GAS INJECTION

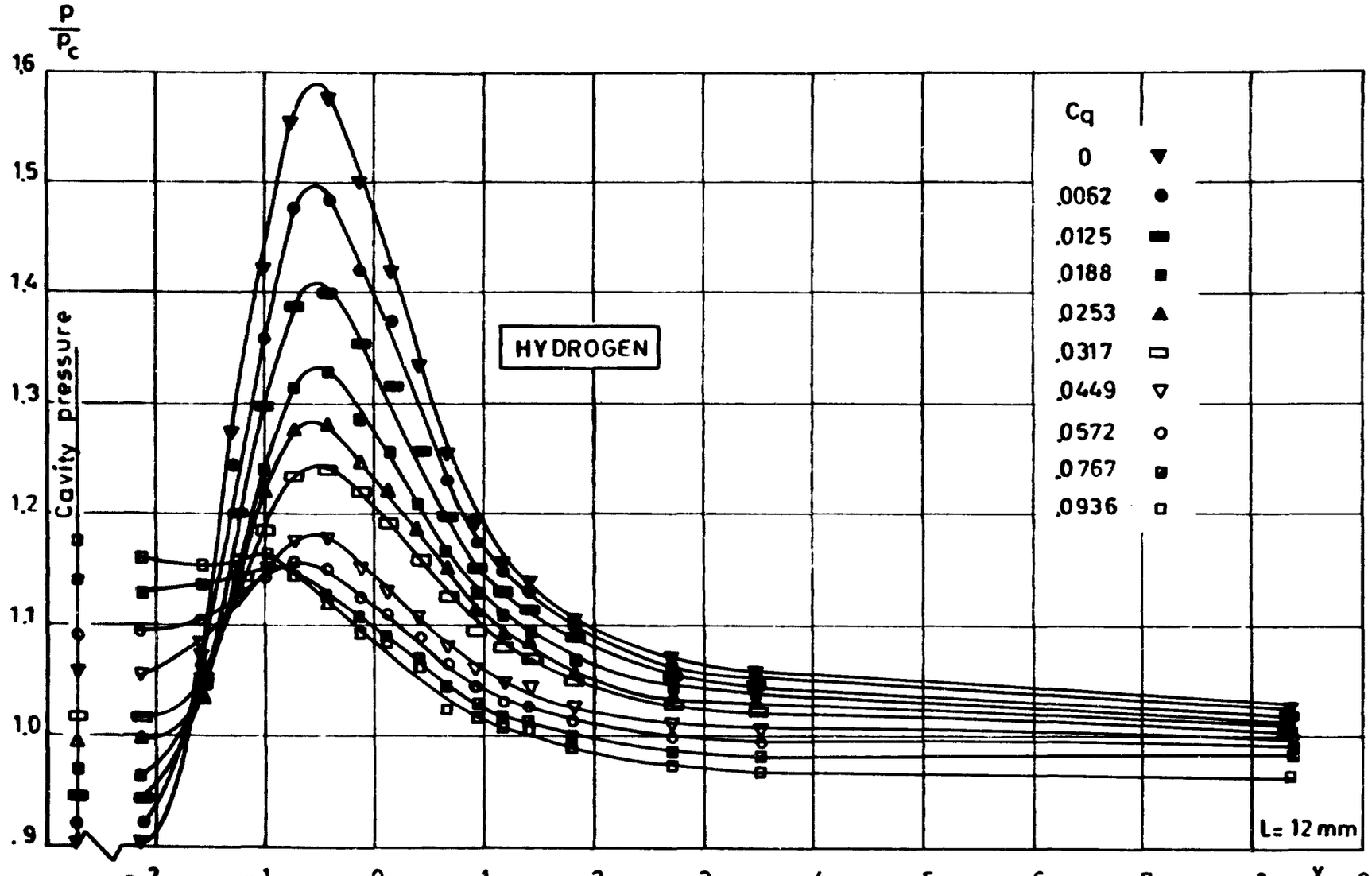

Fig. 3a PRESSURE DISTRIBUTIONS WITH AND WITHOUT GAS INJECTION.

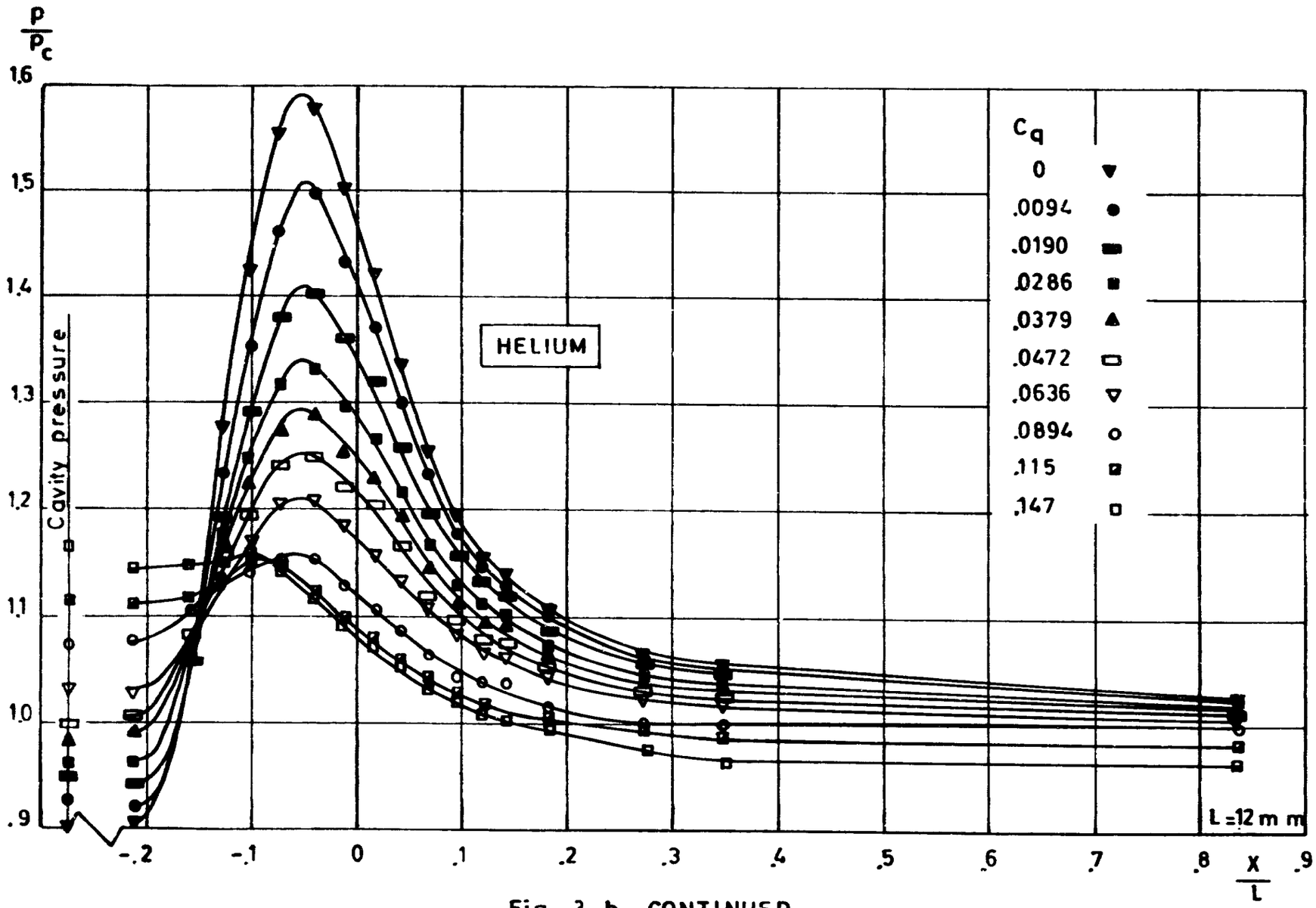

Fig. 3 b CONTINUED.

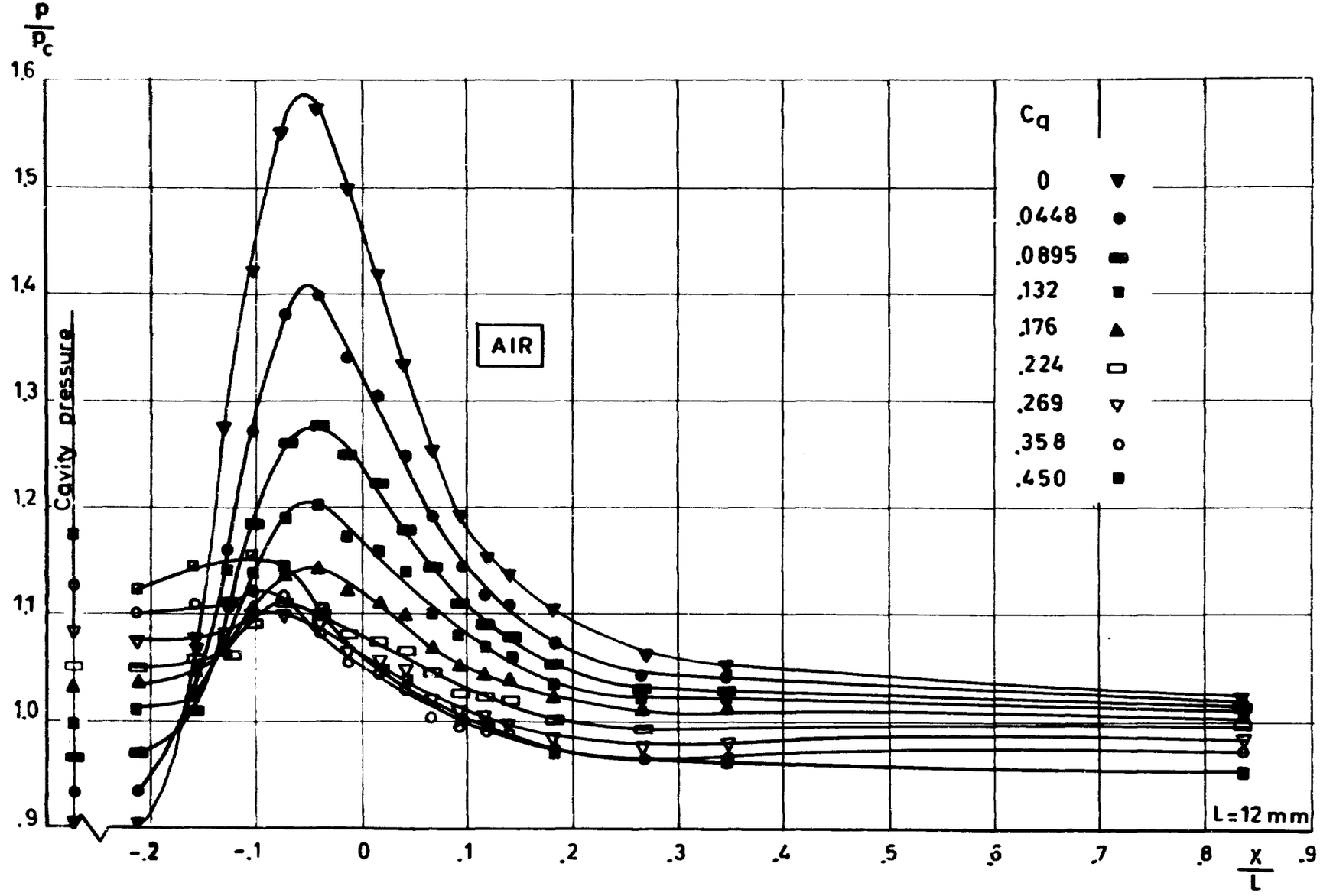

Fig. 3c CONTINUED.

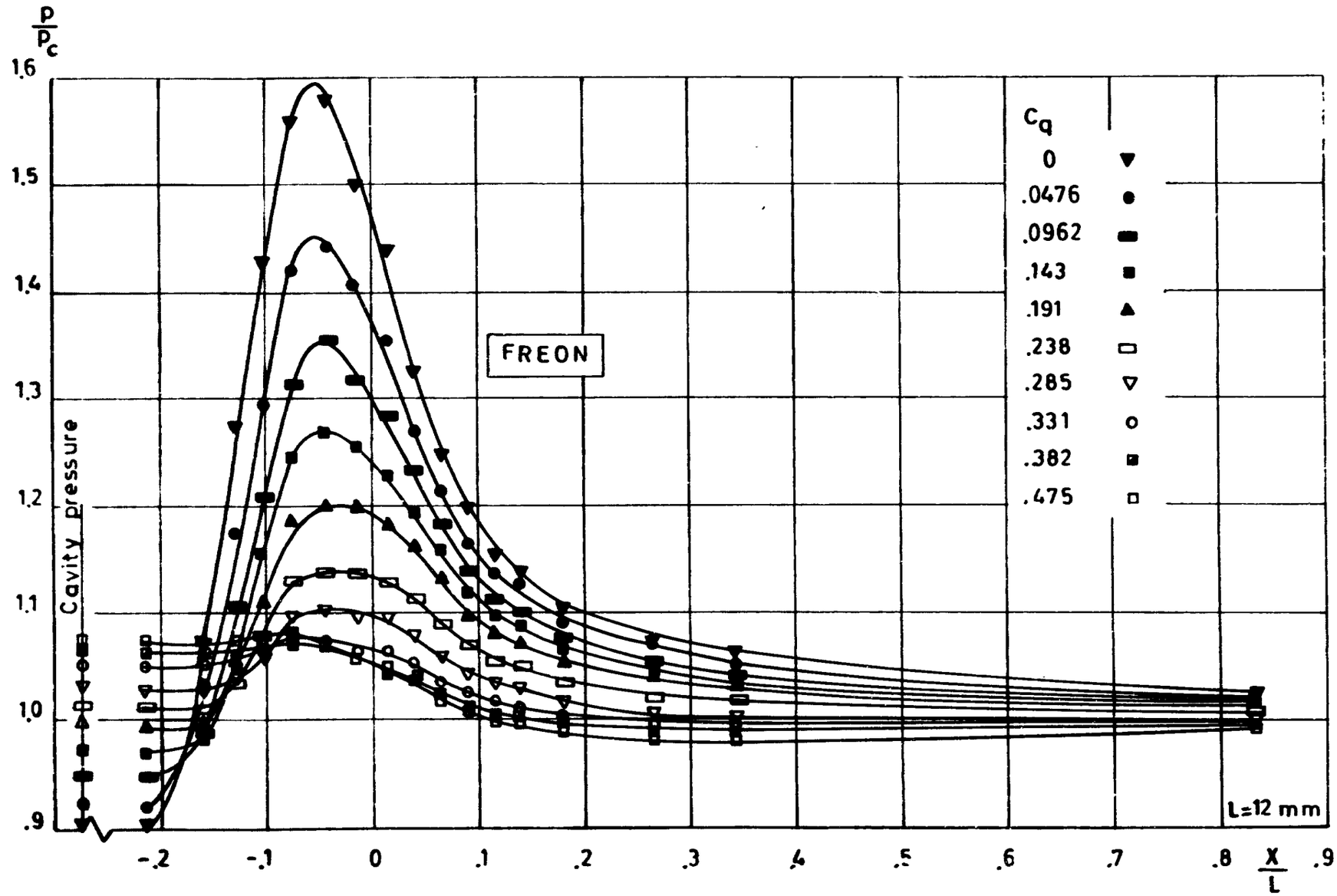

Fig. 3 d CONTINUED.

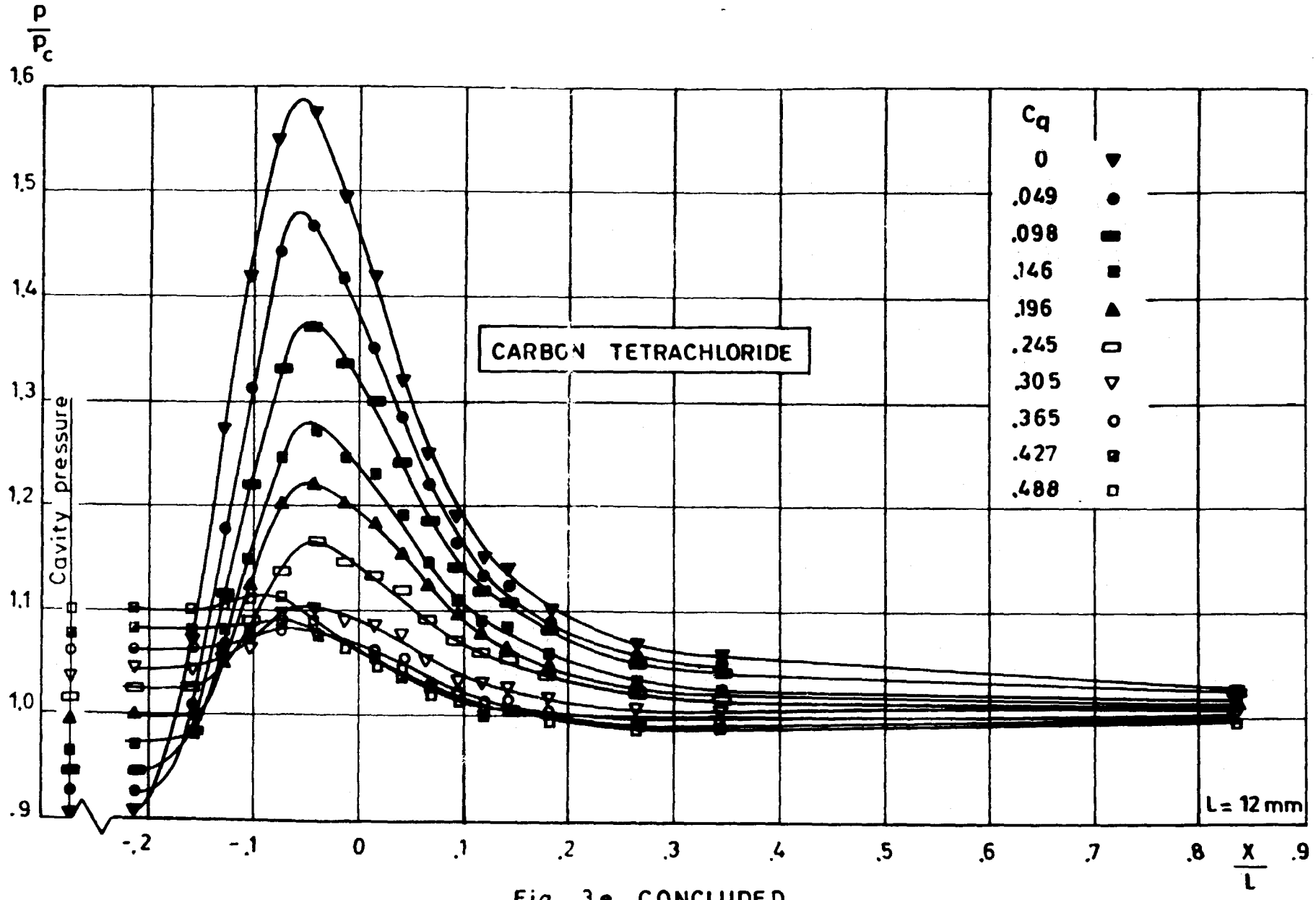

Fig. 3e CONCLUDED.

BEST AVAILABLE COPY

BEST AVAILABLE COPY

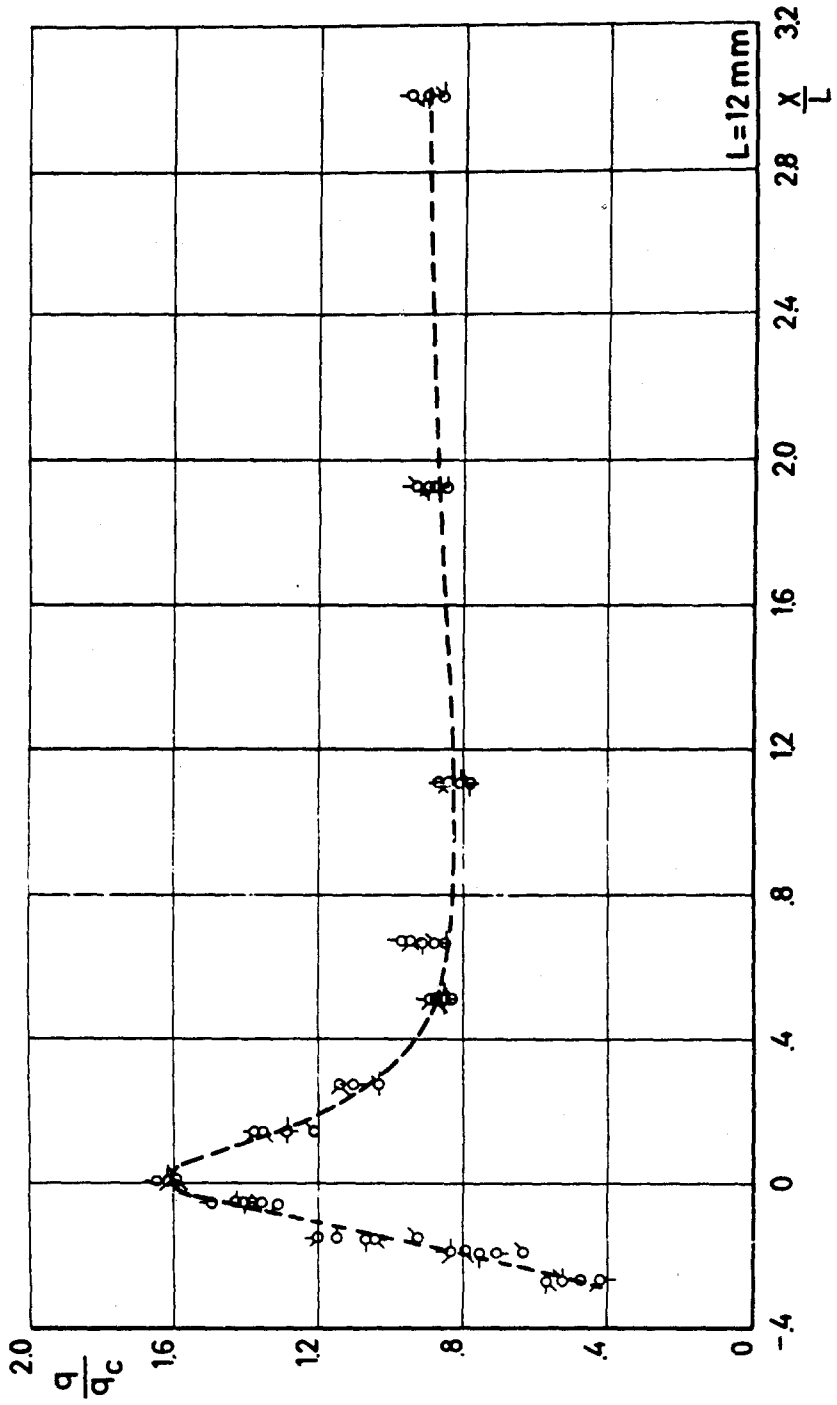

Fig. 4 AVERAGE HEAT TRANSFER DISTRIBUTION WITHOUT GAS INJECTION.

BEST AVAILABLE COPY

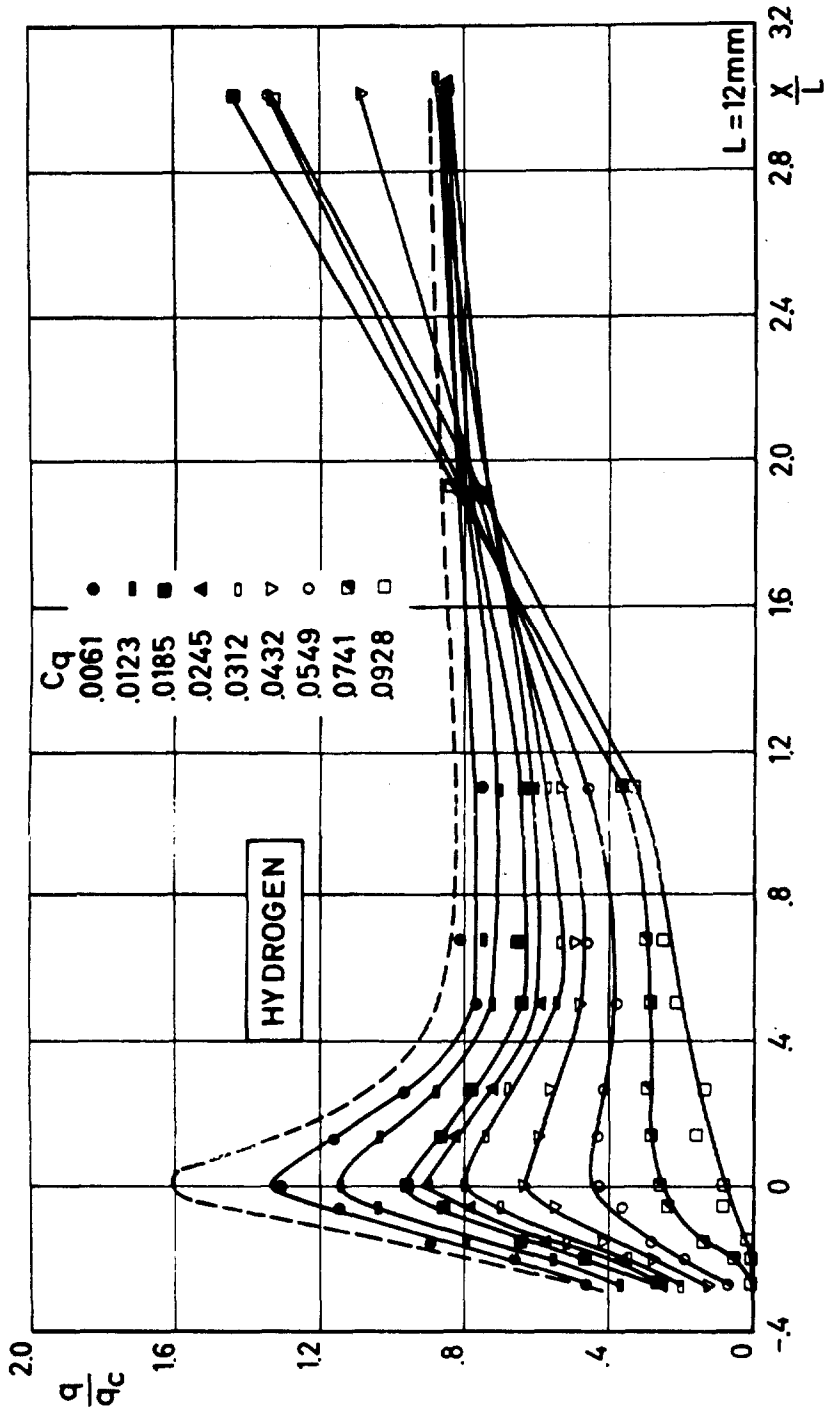

Fig. 5a HEAT TRANSFER DISTRIBUTIONS WITH AND WITHOUT GAS INJECTION.

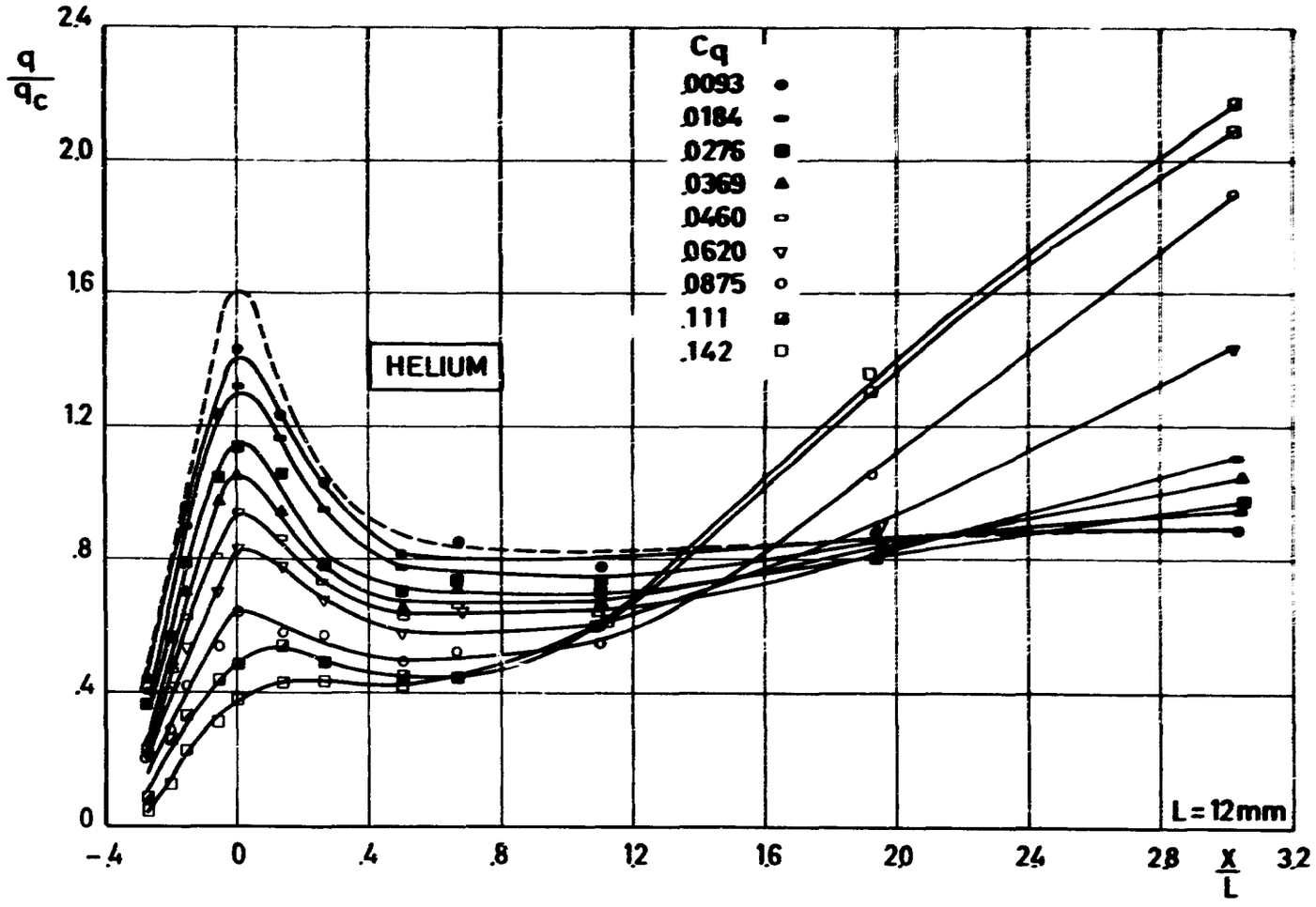

Fig. 5b CONTINUED.

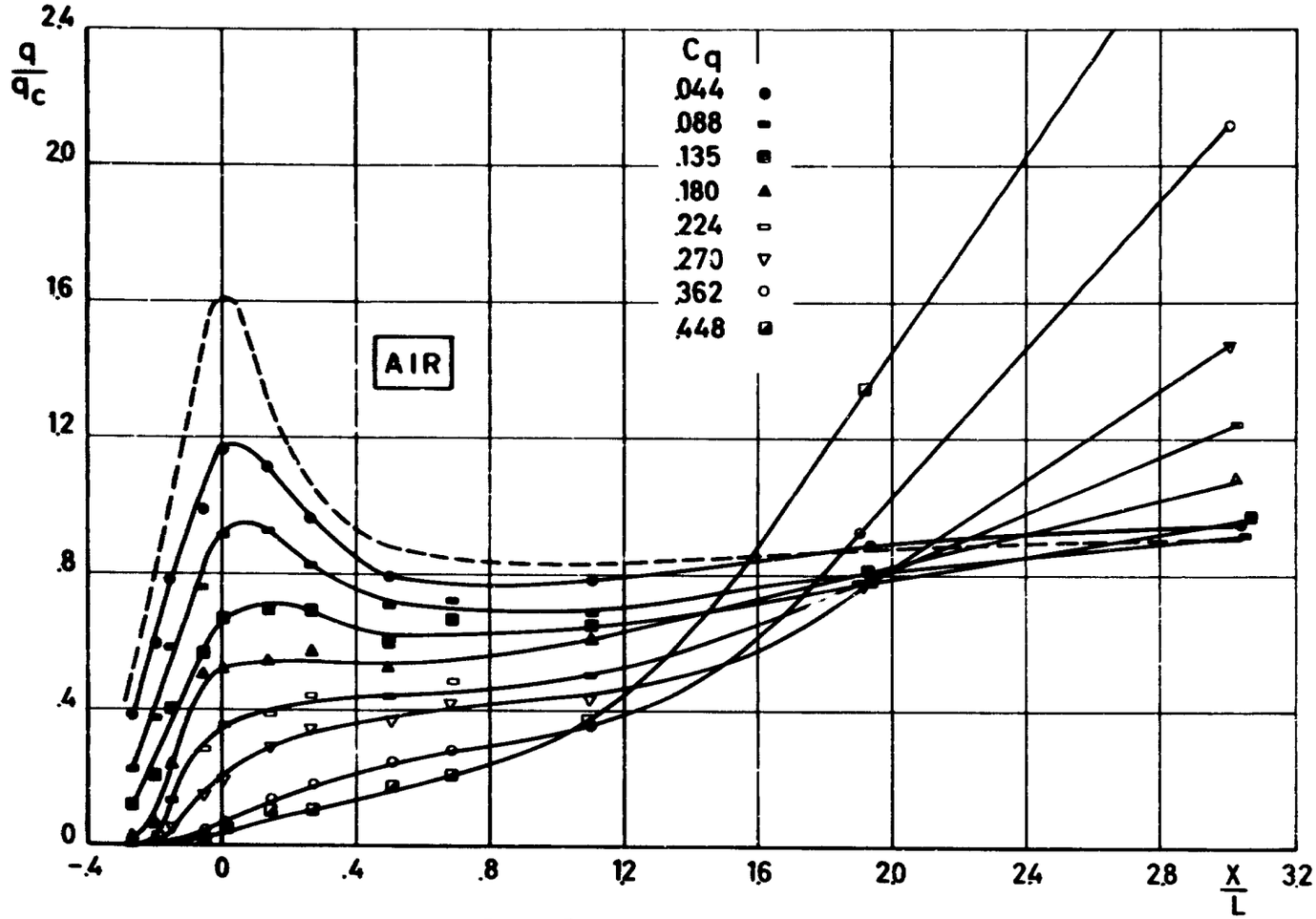

Fig. 5c CONTINUED.

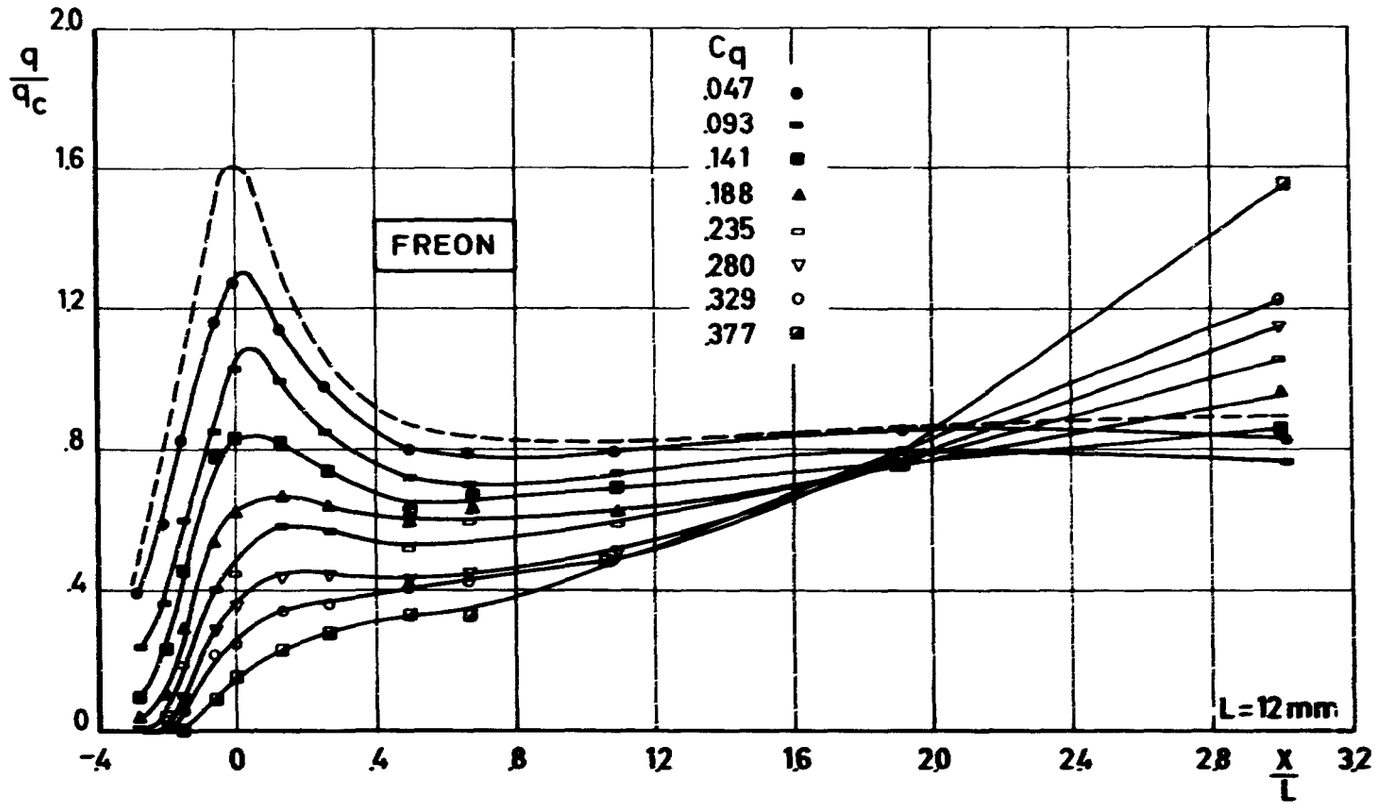

Fig. 5d CONCLUDED.

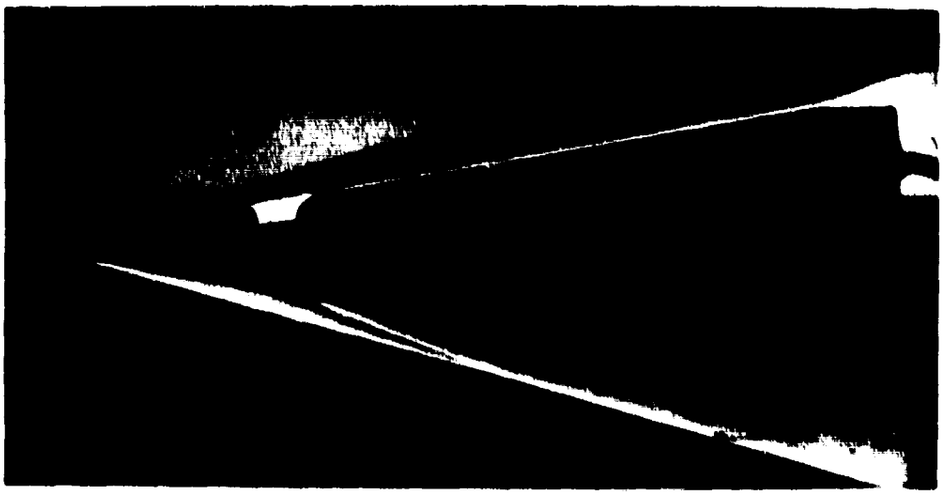

a) Cq = 0

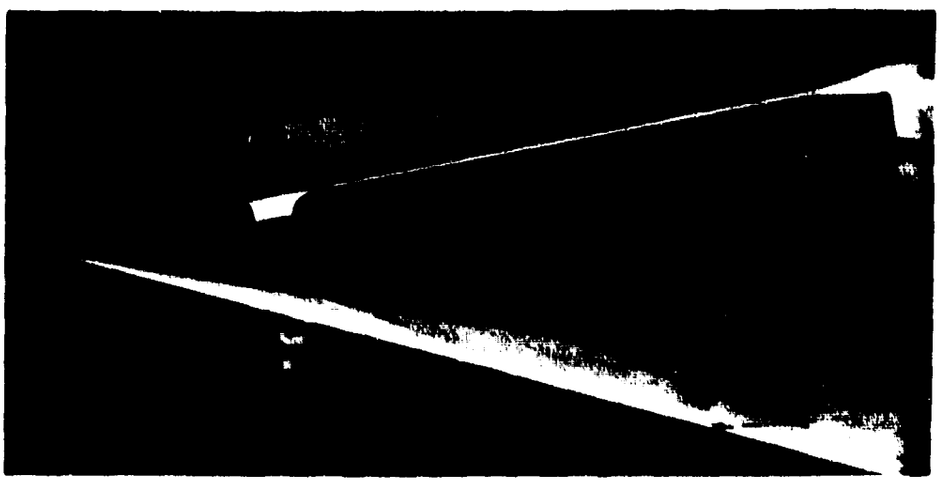

b) Cq = 0.14

Fig. 6 - SCHLIFREN PHOTOGRAPHS FOR AIR INJECTION

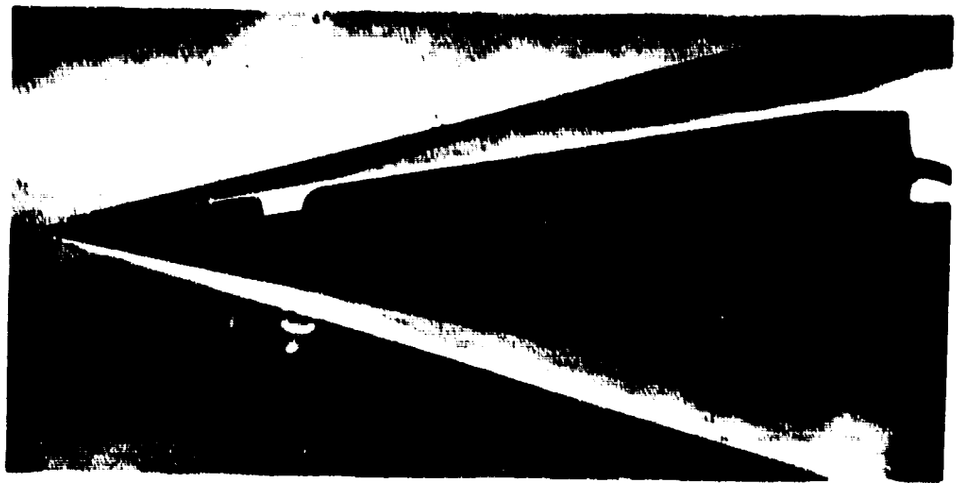

c) $C_q = 0.25$

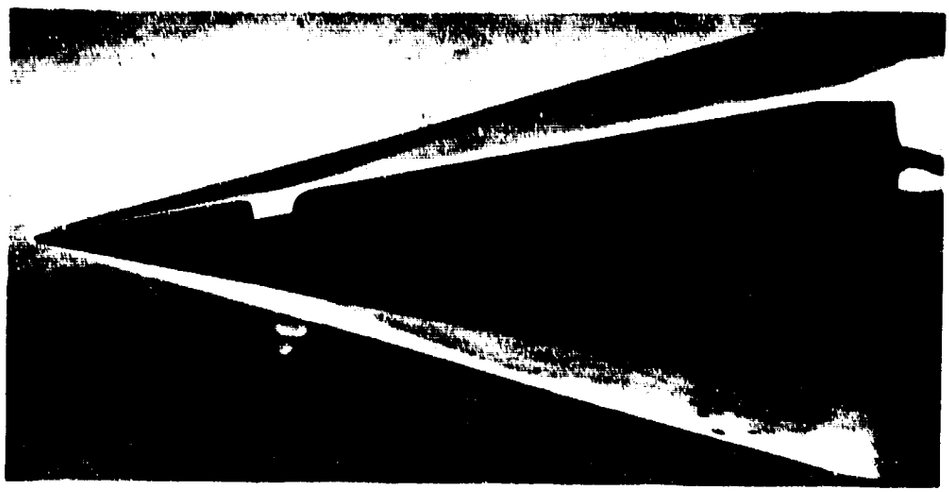

d) $C_q = 0.49$

Fig. 6 - SCHLIEREN PHOTOGRAPHS FOR AIR INJECTION

a) Cq = 0

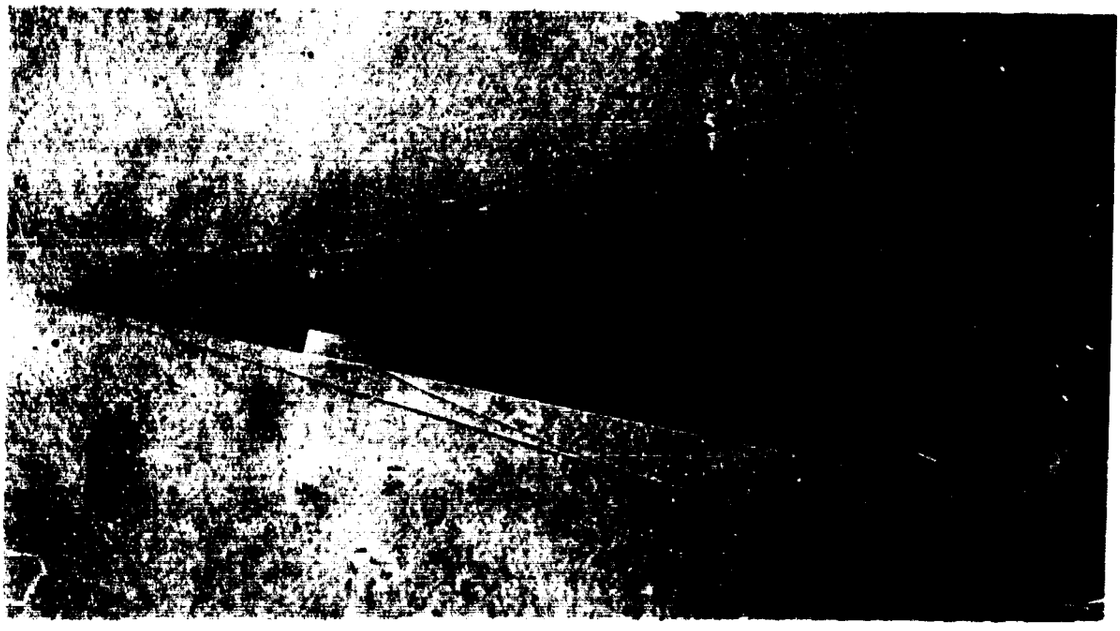

b) Cq = .023

Fig.7- SHADOWGRAPHS FOR AIR INJECTION

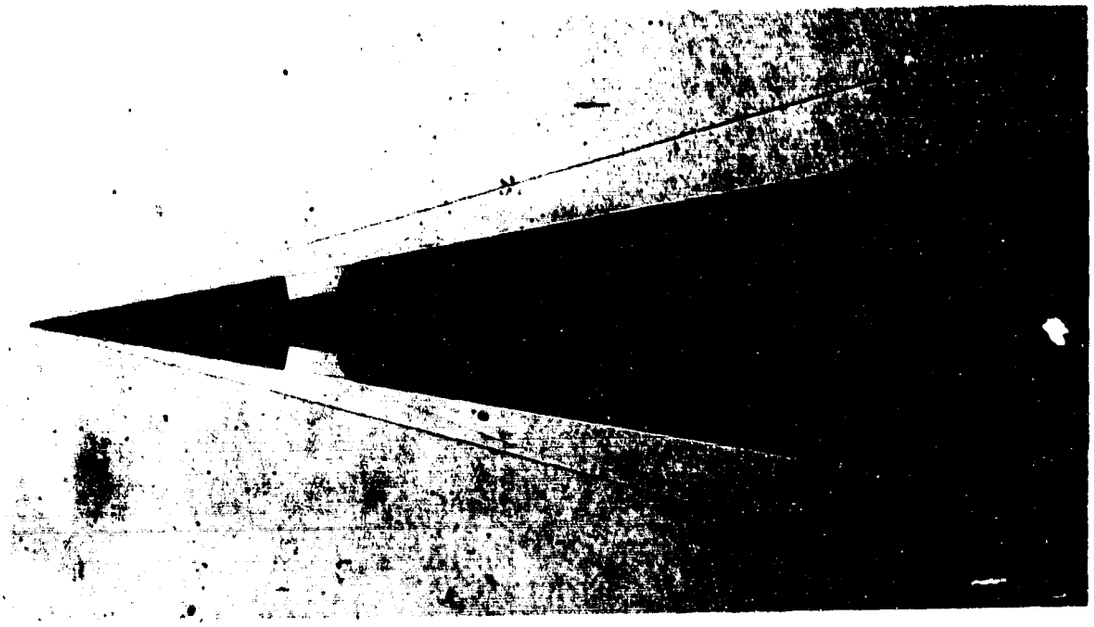

c) Cq = .093

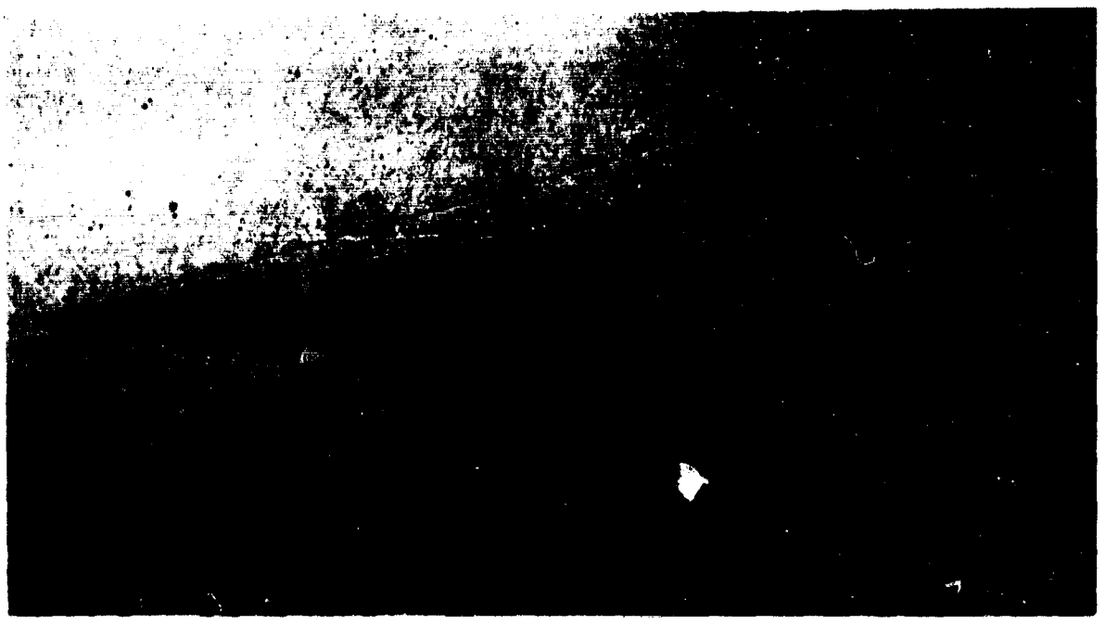

d) Cq = .167

Fig.7 - SHADOWGRAPHS FOR AIR INJECTION

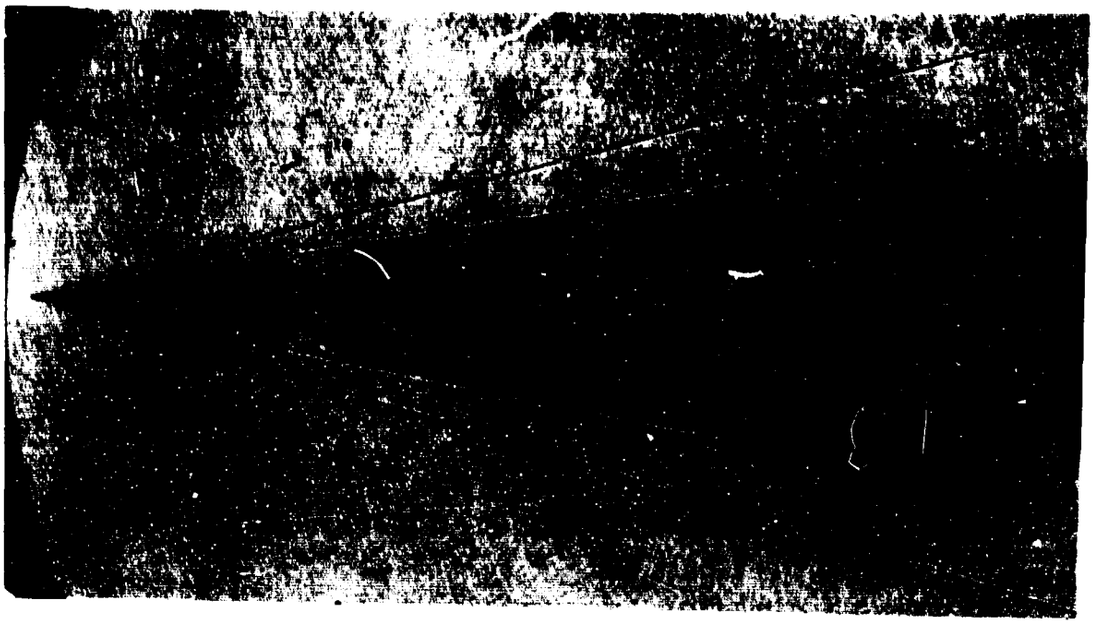

e) Cq = .268

f) Cq = .360

Fig. 7 - SHADOWGRAPHS FOR AIR INJECTION

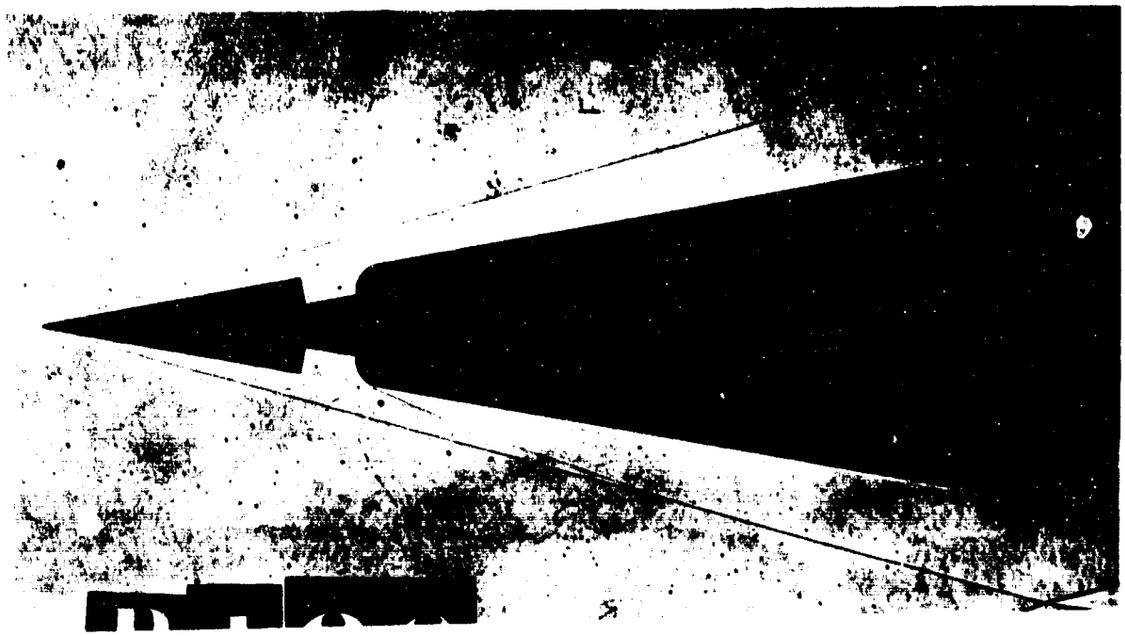

a) Cq = 0

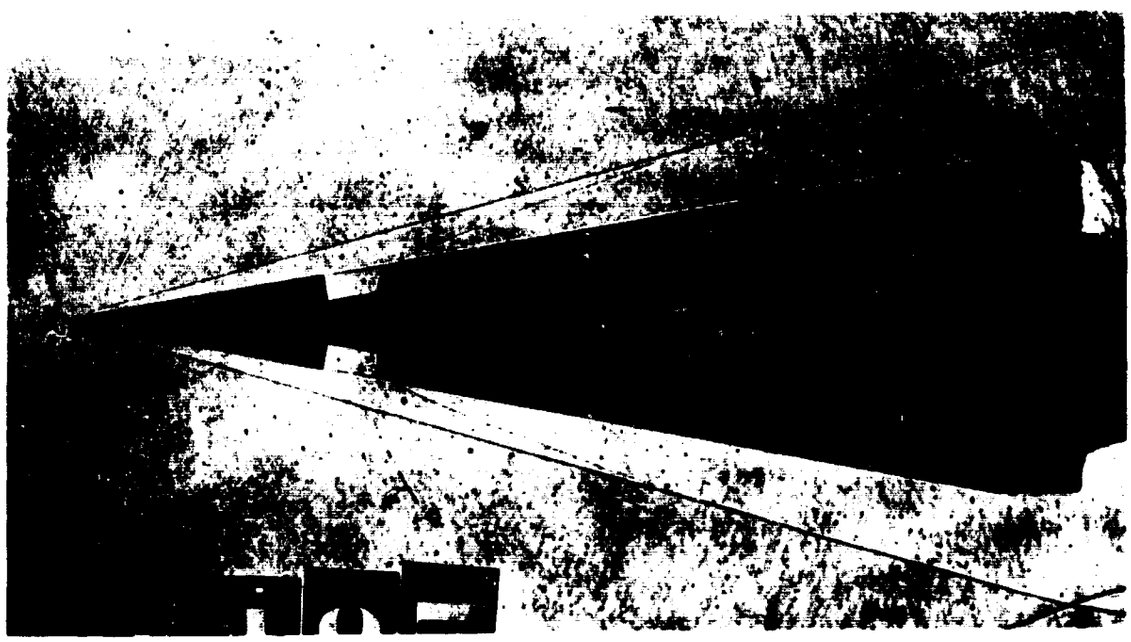

b) Cq =.057

Fig.8 - SHADOWGRAPHS FOR FREON INJECTION

c) C q = .225

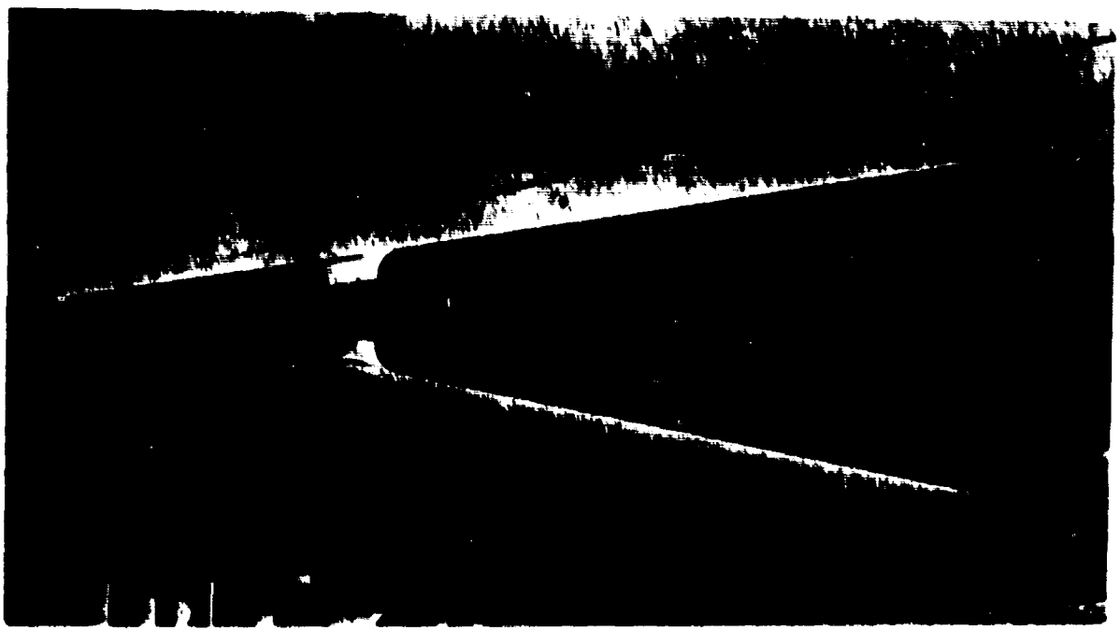

d) C q = .282

Fig. 8 - SHADOWGRAPHS FOR FREON INJECTION

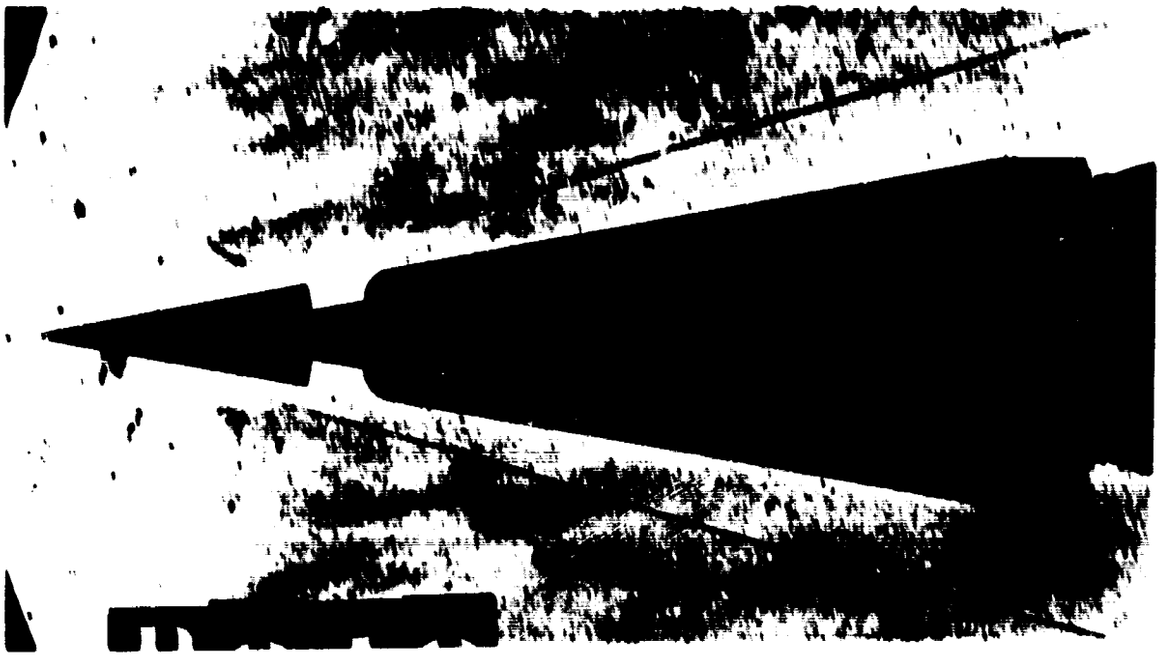

a) Helium injection Cq = .348

b) Enlargement

Fig. 9 - VISUALIZATION OF FLOW UNSTEADINESS

BEST AVAILABLE COPY

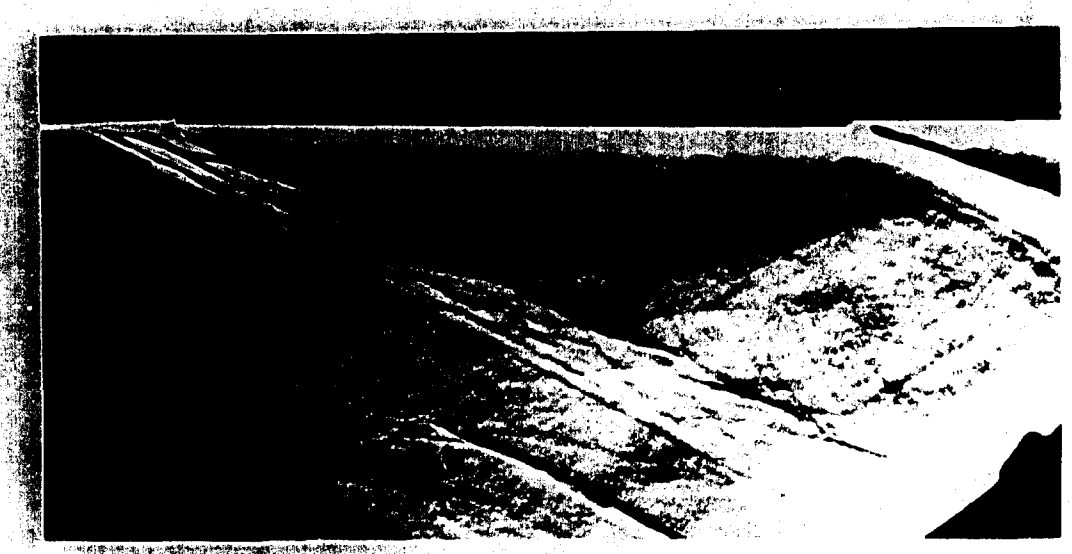

a) Short exposure time

b) Large exposure time

Fig. 10 - SCHLIEREN PICTURES OF A SUPERSONIC FLOW OVER A RECTANGULAR CAVITY

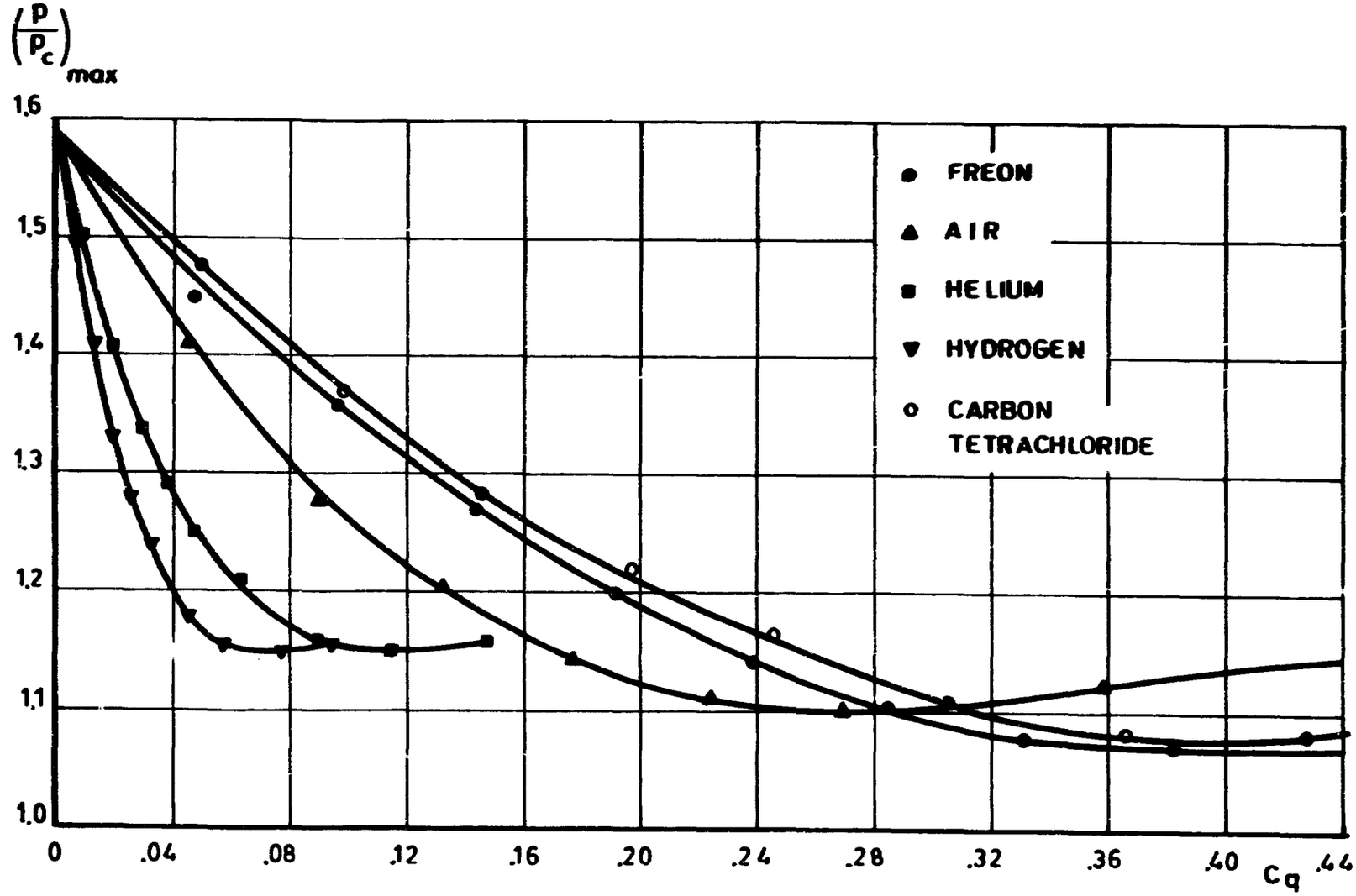

Fig. 11 EFFECT OF GAS INJECTION ON MAXIMUM PRESSURE RATIO.

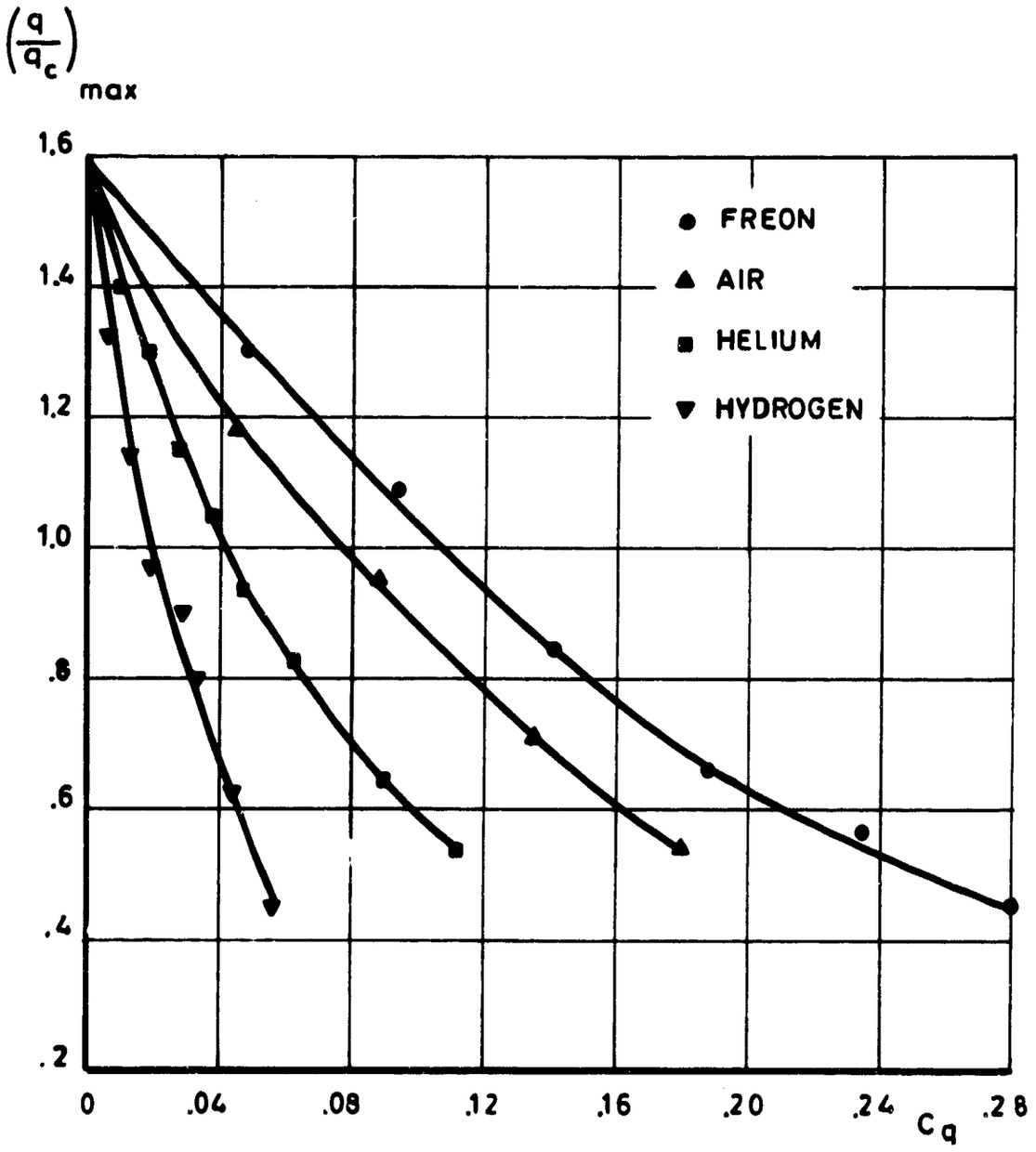

Fig. 12 EFFECT OF GAS INJECTION ON MAXIMUM HEAT TRANSFER RATIO.

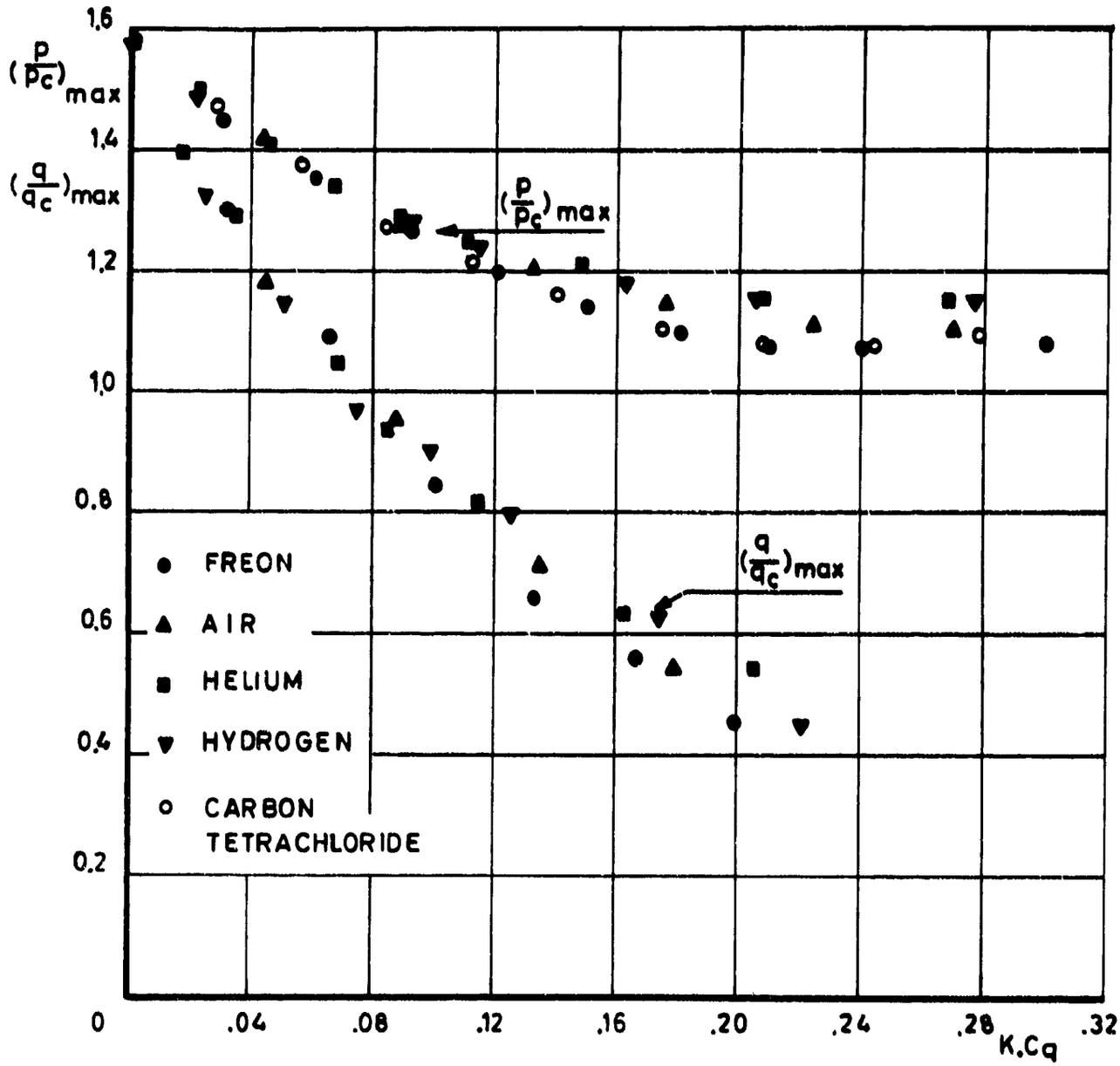

Fig. 13 CORRELATED PRESSURE AND HEAT TRANSFER PEAK RATIOS.

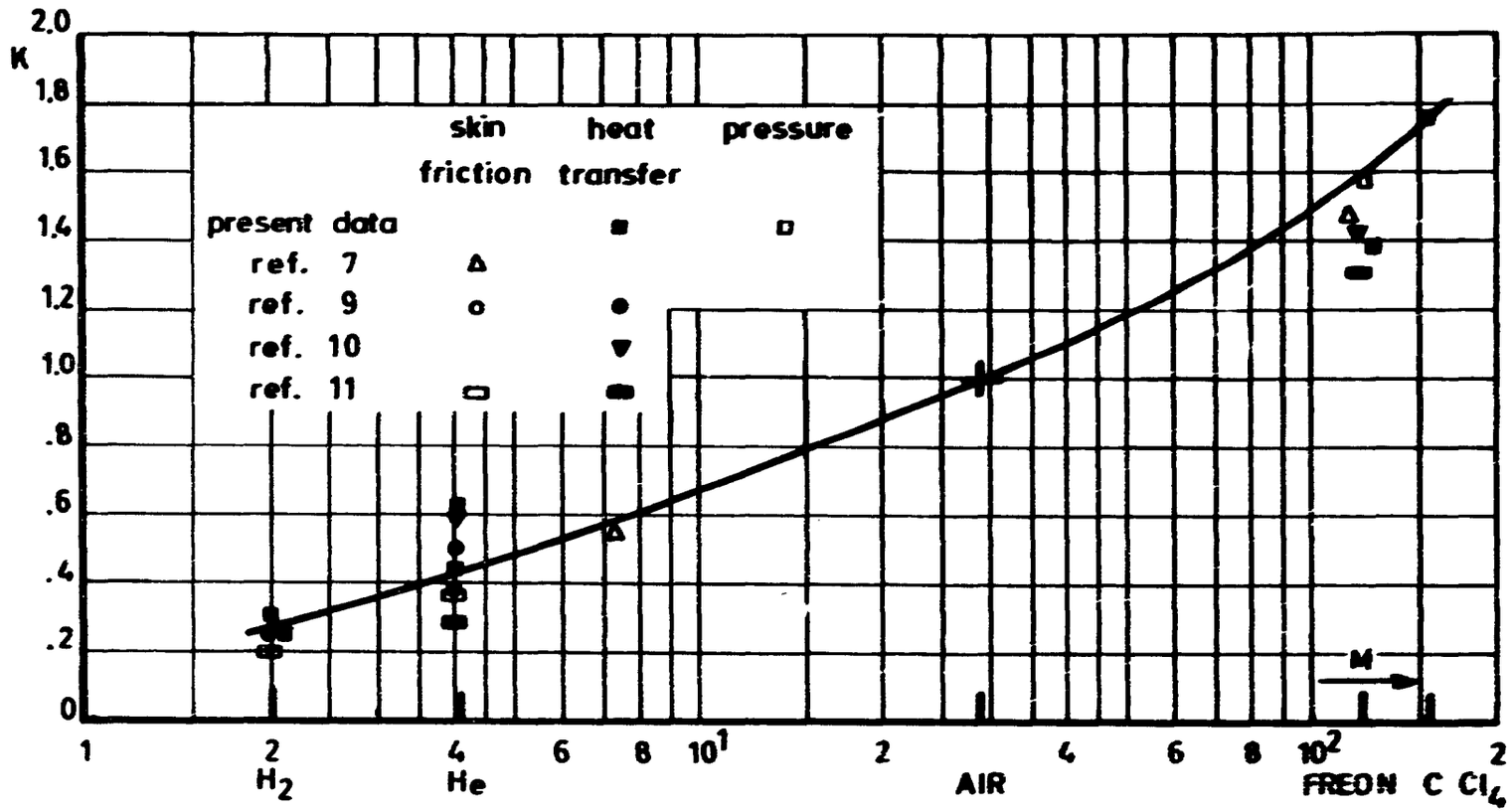

Fig. 14 CORRELATION FACTOR K VERSUS MOLECULAR WEIGHT.

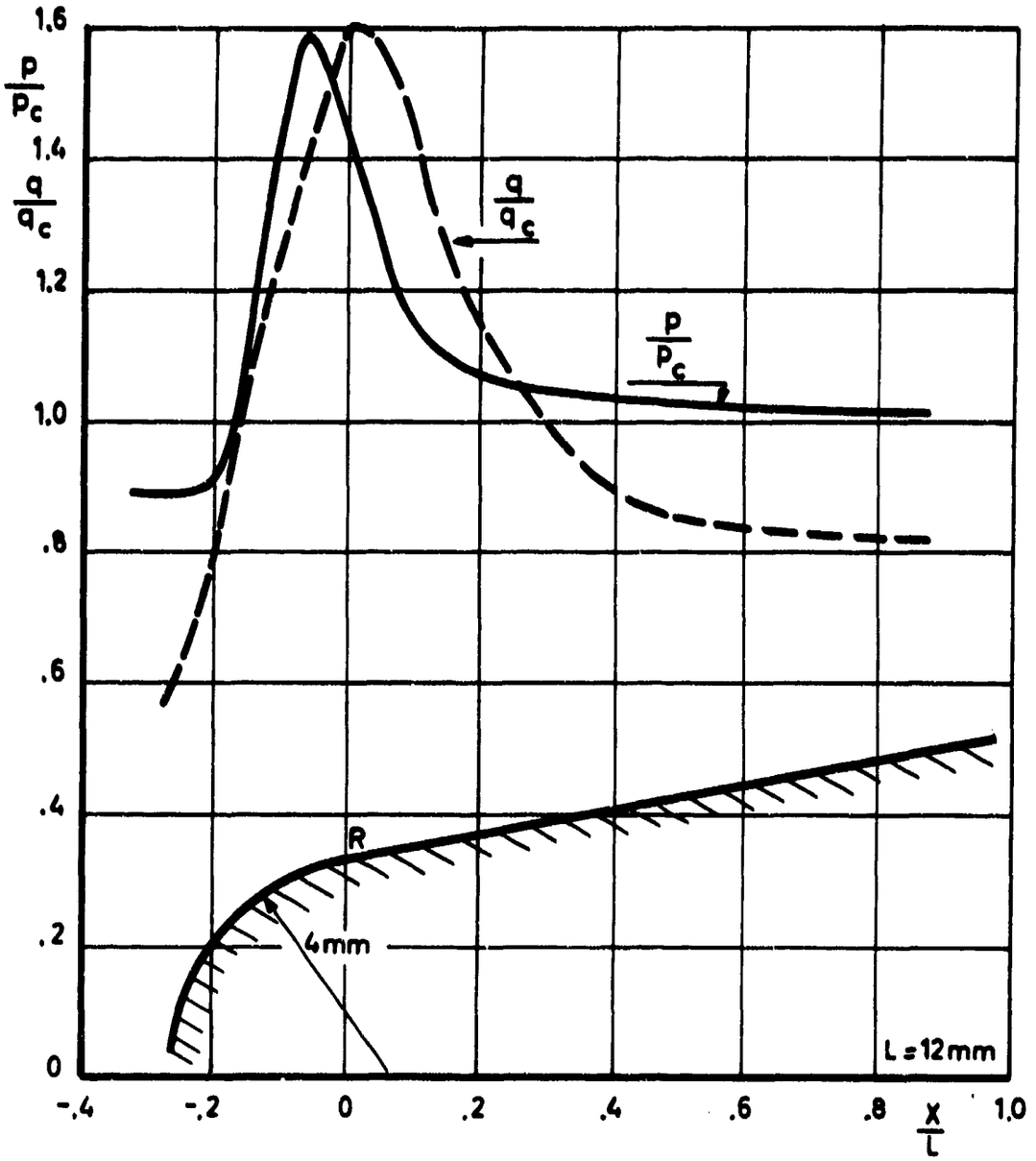

Fig. 15 COMPARISON BETWEEN PRESSURE AND HEAT FLUX DISTRIBUTIONS ($C_q = 0$)

UNCLASSIFIED

Security Classification

DOCUMENT CONTROL DATA - R & D

(Security classification of title, body of abstract and indexing annotation must be entered when the overall report is classified)

1. ORIGINATING ACTIVITY (Corporate author)

von Karman Institute for Fluid Dynamics
High-Speed Laboratory
Rhode-St-Genese, Belgium

2a. REPORT SECURITY CLASSIFICATION

UNCLASSIFIED

2b. GROUP

3. REPORT TITLE

CONE CAVITY FLOW AT M=5.3 WITH INJECTION OF LIGHT, MEDIUM AND HEAVY GASES

4. DESCRIPTIVE NOTES (Type of report and inclusive dates)

Scientific Final

5. AUTHOR(S) (First name, middle initial, last name)

Jean J Ginoux
F Thiry

6. REPORT DATE	7a. TOTAL NO. OF PAGES	7b. NO. OF REFS
November 1968	52	11

8a. CONTRACT OR GRANT NO. EOOAR-68-003

b. PROJECT NO. 9781-02

c. 6144501F

d. 681307

9a. ORIGINATOR'S REPORT NUMBER(S)

[redacted]

9b. OTHER REPORT NO(S) (Any other numbers that may be assigned this report)

AFOSR 69-0168TR

10. DISTRIBUTION STATEMENT

1. This document has been approved for public release and sale; and its distribution is unlimited.

11. SUPPLEMENTARY NOTES

TECH, OTHER

12. SPONSORING MILITARY ACTIVITY

AF Office of Scientific Research (SREM)
1400 Wilson Boulevard
Arlington, Virginia 22209

13. ABSTRACT

The effect on the reattachment pressure and heat transfer peaks of injection of air and foreign gases into the separated region of the laminar flow over a cone cavity model has been investigated at M=5.3.

Injection has generally a favorable effect in reducing these peaks, light gases being more effective. A correlation factor is given to relate together the effects of various gases. A surprizing similarity is found with theoretical and experimental results for unseparated flows over porous walls. Occasionally, very high frequency flow unsteadiness has been observed.

DD FORM 1473

UNCLASSIFIED

Security Classification

BEST AVAILABLE COPY

14 KEY WORDS	LINK A		LINK B		LINK C	
	ROLE	WT	ROLE	WT	ROLE	WT
Separation						
Laminar Flow						
Hypersonic Speeds						
Mass Injection						
Foreign Gas						
Static Pressure						
Heat Transfer						
Cone-Cavity Models						

BEST AVAILABLE COPY